

POLITECNICO DI MILANO
Scuola di Ingegneria Industriale e dell'Informazione
Corso di Laurea Magistrale in Ingegneria Energetica



Modeling Liquid-Droplet Evaporation in a Direct Contact Heat Exchanger

Politecnico di Milano, École Polytechnique de Montréal
“Altan Tapucu” Thermohydraulic Laboratory
Montréal, Canada

Tesi di Laurea di:
Franco Cascella (771139)
Relatore: Andrea Lucchini (PhD)

*né dolcezza di figlio, né la pieta
del vecchio padre, né 'l debito amore
lo qual dovea Penelopé far lieta,* 96

*vincer potero dentro a me l'ardore
ch'i' ebbi a divenir del mondo esperto,
e de li vizi umani e del valore;* 99

*ma misi me per l'alto mare aperto
sol con un legno e con quella compagna
picciola da la qual non fui diserto.* 102

Dante, *Inferno*, Canto XXVI, vv 94-102

*To the people I love
nothing else matters. . .*

ACKNOWLEDGEMENTS

This thesis is the result of two years of trying work. Even though its realization has been strenuous, the feeling of accomplishment I have now in fulfilling it is limitless. However, this accomplishment could not have been reached without the help and mostly the trust of the people who supported me over the past two years.

I would like to thank the two universities, the *École Polytechnique de Montréal* and the *Politecnico di Milano*, that allowed me to do the double degree programs between these two institutions. I was not the ideal student to do this, thus, I've always worked hard in order to gain their confidence. I hope to have achieved this task.

Professor Alberto Teysseidou has had a significant role in these two years. His economic help was essential, but not as much as the trust he has had for me from the beginning of my Master's. Though he did not know me two years ago, he accepted me as his student. Since then, he has never stopped believing in me, in my knowledge and in my ability. For this reason, he has always encouraged me – even my ideas that could have been considered unattainable – and never stopped providing me with precious suggestions and advice (not necessarily limited to my work). Thanks to him, I was able to present my project at the Canadian Nuclear Society in Toronto on June 12th and to write a scientific paper.

My thanks also go to my family whose presence has always been strong, in spite of the seven thousand kilometers that divide us. I thank my sister Cinzia, who has forgiven for not being as present in her life as I would like be, to my mother Lidia, who keeps on bearing me showing infinite tolerance, and to my father Cosimo, who has understood my need to leave Bari, even if he would have preferred me to stay.

I thank my relatives in Vancouver, for making me feel less alone in this country; they have always helped me in the moments of need. Thanks to Filomena, Nicla and Generoso Vitucci for their supporting Skype calls, and to my beloved uncle Girolamo Vitucci, whose absence is harder to handle day by day.

I cannot forget to emphasize the help of the people I have met over the past two years. I thank Giovanniantonio Natale, who is not only a colleague who has patiently analyzed my work providing valuable suggestions, but mostly a friend. The moments we have spent together (inside and outside the school) are a significant part of my experience in Montreal. I thank my closest friends, Valeria Galluccio in Montreal and Alessandra Azzena in Milan, for their unconditional moral support. And I thank all those people I am simply grateful to have met here: Giovanni, the first and best roommate ever, Cecilia for our pleasant runs in Mount Royal Park, Paul and Thomas for improving my French by revising everything I wrote and

correcting my pronunciation, Daniel Del Balso for showing how important our friendship was even on Christmas holidays, Madeleine for being by my side in the most difficult moment of my life, Lidia, Elsa, Rami, Rosario, Linda and all the people I am forgetting. A special thanks go to my friends in Bari, who have never forgotten me: seeing them waiting for me at the airport in Bari was one of the most touching moments of my life.

My final thanks go to the person who uncovered my weaknesses, showing how selfish, touchy and insecure I can be. In other words, she saw how afraid I am to fail in life. Nevertheless, she was always close to me and appreciated me in a way I could never have imagined.

ABSTRACT

In the last thirty years, Direct Contact Heat Exchangers (DCHX) have found success in different power engineering applications. In fact, due to their configuration, which allows the direct contact between the hot and cold fluids, it is possible to reach very high mass and energy transfer efficiencies. Despite their high performance, it remains, to this day, difficult to correctly predict the thermal power as a function of plant operation conditions. In fact, this problematic constitutes a fundamental parameter to correctly operate heat exchangers.

In order to study super-critical water choked flow in a super-critical water loop, a heat exchanger of this type has been recently installed in the “Altan Tapucu” Thermo-hydraulic Laboratory. It consists of a fluid mixer called “quenching chamber”, i.e. a vessel where super-heated steam coming from a test section (where choked flow conditions occur) mixes with sub-cooled water. This component can safely work in a wide range of pressures ($5 \text{ bar} < p < 40 \text{ bar}$). However, on the top of the vessel, a nozzle is set so that the cooling water is sprayed into the chamber under the form of tiny droplets (i.e., about $200 \mu\text{m}$ in diameter).

Within the frame work of this Master’s thesis, we developed a thermodynamic model capable of describing the thermal power in the aforementioned DCHX for different working conditions. The main idea is to apply an energy balance to every single droplet in order to evaluate the total heat transfer. In order to do that, we focused our attention on two problems:

- Droplet size:** to perform any energy balance, it is necessary to know the droplet size, however, the quenching chamber working conditions affect this parameter. That is, the droplet dimensions vary depending on steam pressure, liquid flow rate and temperature. Moreover, for a given condition, droplets are expected to have non-uniform dimensions. This means that firstly, a statistical distribution describing the droplet size is to be found, and secondly, the working conditions have to be considered when evaluating this statistical law.
- Heat transfer:** Since there is a mutual interaction between the sub-cooled liquid (disperse phase) and the super-heated steam (continuous phase), we analyzed two heat transfer modes: convection and evaporation. However, this study cannot be performed without a preliminary evaluation of the droplet velocity. That is, the velocity field needs to be known since it affects the amount of energy released.

In this work, the experimental data collected at École Polytechnique de Montréal are compared with the predictions of our model. We found a very good agreement for steam

pressures of 1.6 and 2.1 *MPa* however, at higher pressures, it over estimates the experimental trends. Hence, we performed an analysis in order to explain the model behavior. Thus, we have justified the observed over predictions at high pressure due to physical variables which are not taken into account in the model (such as droplet collision and break-up).

Despite the fact that our modeling approach may be questionable on several points, it gives us the possibility to analyze the quenching chamber behavior by linking the dynamics of liquid droplets to the total thermal power. This way, we are able to predict some working conditions that may optimize the thermal power in our DCHX. However, this aspect has not been proven yet and should be the research subject of a future work.

RÉSUMÉ

Negli ultimi 30 anni gli scambiatori di calore a contatto diretto (*Direct Contact Heat Exchanger*, DCHX) hanno riscontrato grande successo in diverse applicazioni ingegneristiche. Infatti, in questi scambiatori vi è contatto diretto tra il fluido caldo e fluido freddo, il che permette di ottenere elevati rendimenti energetici. Nonostante le loro elevate prestazioni, è ancora molto difficile valutare gli scambi termici in funzione delle condizioni di funzionamento dello scambiatore di calore; questa valutazione risulta quindi necessaria per garantire il corretto funzionamento dei suddetti DCHX.

Per studiare l'evoluzione fluidodinamica del vapore supercritico e supersonico in una strozzatura (comunemente chiamata *choked flow* in letteratura), un DCHX è stato recentemente installato nel laboratorio di termo-idraulica "Altan Tapucu" dell'École Polytechnique de Montréal. Questo componente, comunemente chiamato *quenching chamber*, consiste in un condotto dove vapore surriscaldato proveniente da una sezione di prova (in cui si verificano le condizioni supersoniche) è mescolato con acqua sotto raffreddata. Questo componente può lavorare in tutta sicurezza in una vasta gamma di pressioni ($5 \text{ bar} < p < 40 \text{ bar}$). Inoltre, sulla parte superiore dello scambiatore, è presente un nebulizzatore (*spray nozzle*) che consente il cambio di fase dell'acqua da continua a dispersa; le gocce d'acqua così formate hanno un diametro dell'ordine di $200 \mu\text{m}$.

Negli ultimi due anni abbiamo sviluppato un modello termodinamico per descrivere lo scambio termico nel DCHX per diverse condizioni di lavoro. L'idea principale è quella di applicare un bilancio energetico per ogni goccia al fine di valutare la potenza termica totale scambiata. Per fare questo, abbiamo focalizzato la nostra attenzione su due questioni:

- Determinazione della dimensione delle gocce:** per effettuare il bilancio energetico, è necessario conoscere la dimensione delle gocce. Tuttavia, le condizioni di lavoro della camera influenzano questo parametro; infatti la dimensione delle gocce varierà a seconda di determinate variabili, quali la tensione di vapore, la portata e la temperatura del liquido. Inoltre, per una data condizione, è impossibile (o perlomeno poco probabile) aspettarsi che gocce abbiano dimensione uniforme. Quindi, bisogna introdurre una distribuzione statistica (*Droplet Distribution Function*, DDF) che da un lato descriva la dimensione delle gocce, dall'altro, tenga conto dell'influenza che le condizioni di lavoro del DCHX hanno sulla suddetta distribuzione.
- Soluzione del problema di scambio termico:** Dal momento che vi è una mutua interazione tra il liquido sotto-raffreddato (fase dispersa) e vapore surriscaldato (fase continua), abbiamo analizzato due modalità trasmissione del calore: convezione ed

evaporazione. Tuttavia, questo studio non può essere eseguito senza una precedente valutazione della velocità delle gocce. In altre parole, la soluzione del problema di scambio termico non può precludere la valutazione del campo di velocità delle gocce, visto che quest'ultimo influenza il trasferimento di calore.

In questo lavoro, i dati sperimentali raccolti presso i laboratori dell'*École Polytechnique de Montréal* sono confrontati con le previsioni del nostro modello. Abbiamo trovato un ottimo accordo per le pressioni della camera di 1.6 e 2.1 *MPa*, ma a pressioni più elevate il modello sovrastima sensibilmente i dati sperimentali. Pertanto, abbiamo effettuato un'analisi per capire le ragioni di questo comportamento: i fenomeni che non sono stati considerati e che possono influire sul modello sono legati alle mutue interazioni fisiche e dinamiche fra le gocce (ovvero la collisione e il *breakup* delle suddette).

Anche se il nostro approccio teorico può essere discutibile su diversi punti, questo modello ci dà la possibilità di analizzare il comportamento dello scambiatore di calore, correlando la dinamica delle gocce alla potenza termica totale scambiata. Nonostante ci siano ancora ampi margini di miglioramento, possiamo ritenerci più che soddisfatti dei risultati ottenuti.

TABLE OF CONTENTS

DEDICATION	iii
ACKNOWLEDGEMENTS	iv
ABSTRACT	vi
RÉSUMÉ	viii
TABLE OF CONTENTS	x
LIST OF TABLES	xii
LIST OF FIGURES	xiii
LIST OF APPENDICES	xv
LIST OF ACRONYMS AND SYMBOLS	xvi
CHAPTER 1 INTRODUCTION	1
1.1 Direct Contact Heat Exchangers (DCHX)	1
1.2 Problem Studied	2
1.3 Research Objectives	4
1.4 Thesis Plan	5
CHAPTER 2 LITERATURE REVIEW	7
2.1 Droplet Size Evaluation	7
2.1.1 The Atomization Process	8
2.1.2 Droplet Distribution Function (DDF)	9
2.2 Heat and Mass Transfer from Liquid Droplets	11
CHAPTER 3 THE EXPERIMENTAL FACILITY	14
3.1 The Super Critical Water Loop (SCWL)	14
3.2 The Test Section	16
3.3 The Quenching Chamber	18

CHAPTER 4	DEVELOPMENT OF A STATISTIC DISRIBUTION FUNCTION FOR THE DROPLET SIZE	21
4.1	The Sauter Mean Diameter	21
4.1.1	Lefebvre's Correlation (1989)	24
4.2	The Droplet Distribution Function	25
4.2.1	The Rosin-Rammler Equation	26
4.3	Considerations on Statistical Methodology	27
CHAPTER 5	HEAT TRANSFER STUDY	30
5.1	The Steam Temperature	30
5.2	The Solution of the Heat Transfer Problem	32
5.2.1	Droplet Convective Heat Transfer	33
5.2.2	Droplet Evaporation Heat Transfer	36
5.3	Thermal Power Transferred in DCHX Systems	37
5.4	Final Remarks on the Presented Procedure	38
CHAPTER 6	RESULTS	40
6.1	Model Methodology	40
6.1.1	Analysis of a DCHX Thermal Condition	43
6.2	Comparison of Model with Experimental Data	47
6.3	Parametric Study	52
6.4	Other Correlation Approach	55
6.4.1	Definition of f	55
6.4.2	Definition of ψ	57
6.5	Final Remarks	59
CHAPTER 7	CONCLUSION	60
7.1	General Objectives	60
7.2	Limits of the Proposed Model	61
7.3	Result Discussion	62
7.4	Usefulness of the Proposed Model	63
7.5	Future Work	64
REFERENCES	66
APPENDIX	68

LIST OF TABLES

4.1	Experimental correlations available in scientific literature	22
6.1	Parameters used to generate Figures 6.2, 6.3 and 6.5	43
6.2	Ratios between predictions and data for three working pressures	57

LIST OF FIGURES

1.1	Example of a DCHX: in a cooling tower, the warm liquid mixes with ambient air. A portion of the water brings the air to saturation, and the rest goes in a container at the bottom of the cooling tower (cooling tower in Dresden, Germany)	2
1.2	Scheme of the quenching chamber: water at conditions 1 passes through the spray nozzle and mixes with steam at conditions 2. Finally, saturated water exits at conditions 3	3
1.3	Thesis plan	6
2.1	Atomization process: formation of ligaments and droplets (adapted from N. Dombowsky and W. R. Johns, <i>Chem. Eng. Sci.</i> , 18, 203–214, 1963)	8
3.1	Flow Diagram	15
3.2	Test section	17
3.3	Test section scheme	18
3.4	(a) Photo of the quenching chamber (b) scheme of the quenching chamber	18
3.5	Spray System catalogue	19
3.6	Spray nozzle components and flow pattern (Spray System Catalog) . .	20
4.1	Location of the characteristic diameters on a given Droplet Distribution Function (DDF)	22
4.2	D_{32} as a function of P_{qch} and \dot{V}_{liq}	25
4.3	Statistical methodology used to evaluate the DDF	27
4.4	Examples of the DDF	28
5.1	Thermodynamic process into the test section	31
5.2	Choked flow experimental data (Muftuoglu and Teyssedou, 2013) . . .	32
5.3	Droplet control volume	34
5.4	Comparison between the real velocity trend and the approximation . .	35
6.1	Model flow diagram	41
6.2	Parametric velocity (in m/s) as a function of time and droplet size . .	44
6.3	Temperature field	45
6.4	Energy released from droplets as a function of residence time	45
6.5	Energy released from droplets as a function of size	47
6.6	Comparison of model predictions with data	48
6.7	Model predictions ($P_{qch} = 1.6 MPa$)	49

6.8	Model predictions ($P_{qch} = 2.1 \text{ MPa}$)	50
6.9	Model predictions ($P_{qch} = 3.1 \text{ MPa}$)	51
6.10	Heat transfer rate as a function of DCHX pressure P_{qch} and q	52
6.11	Heat transfer as a function of quenching chamber pressure P_{qch} and volumetric flow rate \dot{V}_{liq}	52
6.12	Influence of volumetric flow rate \dot{V}_{liq} on predictions	53
6.13	Influence of quenching chamber pressure P_{qch} on predictions	54
6.14	Analysis of the coefficients a , b and c	56
6.15	Evaluation of the correction coefficient (Equation 6.5)	58
6.16	Experimental data and proposed correction on predictions	58
.1	Atomization Process	68
.1	Quenching chamber scheme	76

LIST OF APPENDICES

APPENDIX A	68
APPENDIX B	71
APPENDIX C	74
APPENDIX D	76

LIST OF ACRONYSMS AND SYMBOLS

Alphabet Letters

A_s	Surface area [m^2]
$Bi = \frac{hD}{k_l}$	Biot number
c_p	Heat capacity [$J/(kgK)$]
C_D	Drag coefficient
D	Droplet diameter [m]
$D_{0.1}$	Diameter such that 10% of total liquid volume is in drops of smaller diameter [m]
D_{peak}	Value of D corresponding to the peak of $F(D)$ [m]
$D_{0.5}$	Diameter such that 50% of total liquid volume is in drops of smaller diameter [m]
$D_{0.632}$	Diameter such that 63.2% of total liquid volume is in drops of smaller diameter [m]
$D_{0.999}$	Diameter such that 99.9% of total liquid volume is in drops of smaller diameter [m]
D_{32}	Sauter mean diameter [m]
ΔP	Pressure differential [Pa]
f	Drag Factor
$F(D)$	Cumulative distribution function for droplet size
$Fo = \frac{\alpha t}{R^2}$	Fourier number
FN	Flow Number [m^2]
g	Gravitational acceleration [$9.81m/s^2$]
h	Convective heat transfer coefficient [$W/(m^2K)$]
h_{fg}	Difference between vapor and liquid saturation enthalpies [J/kg]
k	Conductivity [$W/(m^3K)$]
i	Summation index
L	Nozzle length [m]
\dot{m}	Flow Rate [kg/s]
$Nu = \frac{hD}{k_v}$	Nusselt Number
r	Radius [m]
$Re = \frac{\rho Dv}{\mu}$	Reynolds number
p, P	Pressure [bar]

$Pr = \frac{c_p k}{\mu}$	Prandtl number
t	Sheet thickness in Equation 4.6 [m]
t	Time in Equation 5.2 [m]
T	Temperature [$^{\circ}C$]
u	Droplet velocity [m/s]
v	Droplet velocity [m/s]
\mathbf{v}	Relative velocity [m/s]
V	Volume [m^3]

Greek Letters

α	Diffusivity [m^2/s]
Γ	Gamma function
ζ_n	Infinite solutions of Equation 5.9
θ	Spray nozzle cone angle [$^{\circ}$]
ρ	Density [kg/m^3]
μ	Dynamic viscosity [Ns/m^2]
ν	Kinematic viscosity ($\nu = \frac{\mu}{\rho}$) [m^2/s]
σ	Surface tension [J/m^2]
τ	Surface shear stress [Pa]

Subscripts

cr	Critic
D	Droplet
$evap$	Evaporation
$conv$	Convection
g	Gas phase
h	Constant enthalpy
l	Liquid phase
qch	Quenching chamber
s	Constant entropy
sat	Saturation
v	Gas phase

Acronyms

DCHX	Direct Contact Heat Exchanger
DDF	Droplet Distribution Function
SCWL	Super Critical Water Loop

CHAPTER 1

INTRODUCTION

1.1 Direct Contact Heat Exchangers (DCHX)

The use of DCHX is common in modern industries. In fact, compared with ordinary heat exchangers, the energy and mass transfer efficiencies reachable with DCHXs are considerably higher. Their first application dates back to the Industrial Revolution, when James Watt developed a direct contact condenser to be used in his steam engine (Jacobs, 2011). Since then, DCHXs have found great success in many engineering fields.

The reason of this success lies in their configuration: conventional heat exchangers are designed in such a way that the heat is forced to pass through a wall which decreases the overall efficiency. As for in DCHXs, hot and cold working fluids mix together to reach maximum heat and mass transfers. In fact, when studying the heat transfer, because of the lack of a wall that divides the two streams, a thermal resistance related to this wall should not be considered. In effect, this provokes a lower entropy losses than conventional heat exchangers. Also, the heat transfer rate is enhanced by the large contact surface area due to fluid mixing and to phase change, as the case may be. DCHXs are economically competitive too. Their capital cost is low since these heat exchangers do not present any kind of constructive complexity (a DCHX can be simply a vessel, as the one in our laboratory) and, in most cases, they have very compact dimensions. Even the maintenance cost is low; it is sufficient to think of a shell and tube heat exchanger, in which the large contact surface area comes from the high number of tubes crossed together in a complex geometry; during its service, if a replacement part is needed, the cost related to this change may be high. The absence of this complexity in DCHXs clearly explains their low maintenance costs (Jacobs, 2011).

It is possible to find several DCHX configurations, depending on the two phases that the working fluids present. That being said, the heat transfer can occur between gas and liquid phases, between solid and liquid (or gas) phases or between two liquid phases. Another distinction is related to the presence of the phase change of one or both streams. However, the most common configuration involves the heat transfer between gas and liquid phases (Saunders, 1988) with phase change (i.e., evaporative condensers). This kind of DCHXs finds numerous applications in nuclear power plants (cooling towers, Figure 1.1), air-cooling and in petrochemical engineering (Takahashi *et al.*, 2001).



Figure 1.1 Example of a DCHX: in a cooling tower, the warm liquid mixes with ambient air. A portion of the water brings the air to saturation, and the rest goes in a container at the bottom of the cooling tower (cooling tower in Dresden, Germany)

Despite their common use, gas-liquid DCHXs present disadvantages. In fact, on one hand, the mixing of the stream to be cooled and a cooling fluid leads to high heat transfer rates, on the other, it causes some problems. First of all, fluid mixing is not always acceptable; in certain conditions, the hot working fluid must be preserved and it cannot be contaminated by the cooling fluid. Another problematic concerns the choice of the cooling fluid, which has to be done regarding the fact that it cannot be recovered (or separated after mixing). Thus, the use of a DCHX requires a cooling liquid to be available in large quantities and, for this reason, at a low cost (i.e., water). Finally, another difficult problem is the prediction of heat transfer; despite the fact that DCHXs have been used for more than two hundred years, the physical phenomena pertaining to the mixing process are not well understood yet (i.e., different heat transfer modes may occur simultaneously). To this day, reliable heat transfer calculations remain difficult to achieve and in turn, reduces the usage of DCHXs to a few applications.

1.2 Problem Studied

In May 2012, renovations took place in the Thermo-Hydraulic Laboratory of École Polytechnique de Montréal in order to update the thermal loop for which the main purpose is to study super-critical water choked flow (this fluid-dynamic condition will be analyzed in Section 3.2). Presently, this facility is under operation.

At the time of the loop design, regarding the need to cool steam, it was decided to include a DCHX similar to the ones described above. The design consists of a quenching chamber in which super-critical water mixes with sub-cooled liquid droplets (i.e., of about $200\ \mu\text{m}$ in diameter) coming from a spray nozzle (Figure 1.2). Consequently, a control system

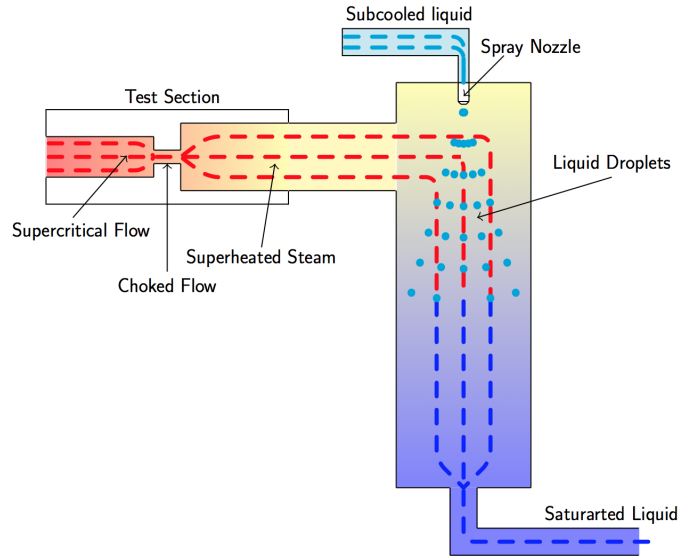


Figure 1.2 Scheme of the quenching chamber: water at conditions 1 passes through the spray nozzle and mixes with steam at conditions 2. Finally, saturated water exits at conditions 3

able to predict the optimum cooling-liquid flow rate is needed. Although it is a mandatory requirement to insure an appropriate operation of the DCHX, the development of the control system is not an easy task. This difficulty is not only caused by the problems related to their design, as mentioned in the previous section, but also due to different phenomena related to the operation of the quenching chamber. To this aim it is necessary to know:

- **Steam conditions not exactly known** before entering in the quenching chamber, the super-critical water passes through a test section, in which choked flow is performed (Figure 1.2). Since the nature of the transformation occurring in the test section is not thermodynamically known, it is not possible to exactly predict the conditions of the steam at the quenching chamber inlet (even if its conditions are accurately known at the test section inlet).
- **Difficulties in predicting droplet size** the spray nozzle present in the quenching chamber is a fundamental component. In fact, it converts the cooling liquid from a continuous to a disperse phase in a complex process called atomization. That being said, the water enters into the DCHX under the form of droplets (Figure 1.2). In order

to evaluate the droplet dimension, a parameter needed to find the heat transfer, a deep knowledge of the factors that influence the atomization quality (which are geometric characteristics of the nozzle, liquid flow rate, quenching chamber pressure and steam temperature) is needed (Schick, 2006). Moreover, even if a qualitative analysis on atomization is made, it is not realistic to expect droplets with uniform sizes. Thus, a procedure that takes into account the complexity of the atomization process and is capable of finding a statistical distribution for droplet size is needed.

- **Heat transfer** since sub-cooled water blends with super-critical water, it is natural to think that two heat transfer modes occur, i.e. convection (until the liquid and/or steam temperatures reach saturation conditions) and phase change (liquid evaporation and/or steam condensation). Convection heat transfer is not easy to estimate because an analysis on heat transfer yields two kinds of convection. The first one occurs through the steam boundary layer, on the surface of the droplet, and the second occurs in the droplet itself, since the temperature gradient inside it gives rise to convective liquid movements (Celata *et al.*, 1991). Even the phase change problem is not easy to solve; because of the mutual exchange of heat between hot and cold fluids (due to the mixing), it is not possible to predict what kind of phase change will predominate. It may be evaporation of liquid droplets or condensation of steam. Moreover, convection heat transfer and phase change may happen simultaneously, making the heat transfer problem that much more difficult to solve.

These are only a few of the problems that can occur when predicting the thermal power exchanged in the quenching chamber. Some of them can be encountered for other configurations of DCHXs, which adequately explains why, the use of these heat exchangers is not common despite their great performance.

In this work, a thermodynamical and physical model able to describe the DCHX is presented. The aim of this model is to evaluate the heat exchange in order to find the cooling-liquid flow rate. The aforementioned phenomena have been studied, but, since taking them into account leads to a highly complex problem, simplifying hypotheses have been made and will be presented through the course of this thesis.

1.3 Research Objectives

Over the past two years, a model for the quenching chamber showed in Figure 1.2 has been developed at École Polytechnique de Montréal. Its main goal is to evaluate the heat transfer rate for different working conditions. In order to do that, it is implemented with

MatLab¹, to compute:

1. The Droplet Distribution Function (DDF), considering that the atomization depends firstly, on the geometrical characteristics of the nozzle (fixed, since the spray nozzle cannot be changed), and secondly, on the working conditions (variables such as the liquid flow rate, the quenching chamber pressure and the steam temperature);
2. The heat transfer problem, since the initial droplet size is known; the following information is needed: the droplet size (i.e., when phase change occurs), the drag coefficient, the droplet velocity, the heat transfer coefficient, the temperature and the evaporation rate. These properties have been studied considering that they are functions of the droplet size and of the residence time in the DCHX;
3. The power and the total energy exchanged into the DCHX for a given set of conditions.

Last but not least, an important task is the validation of the code; thus, the predictions are compared with experimental data collected at the Thermo-Hydraulic Laboratory and the results are listed in this thesis as well.

It is important to underline that choked flow has not been analyzed along this work. Even if this phenomenon has a great influence on steam temperature (parameter that is needed to study the heat transfer), choked flow is too complex. In fact, this fluid dynamic condition has been studied by a PhD student and in this work, we use a portion of his research results to validate our hypotheses (Muftuoglu and Teyssedou, 2013) as it will be seen through the course of this work.

1.4 Thesis Plan

The thesis can be divided into three main parts. First of all, a “Theoretic Background” section containing the basic information needed to understand the problems addressed in this document. Secondly, a “Model Description” section in which the code is developed. And thirdly, a “Final Remarks” section where we will draw the conclusions of this study (Figure 1.3). Each chapter of this thesis belongs to one of these sections. In the first part (“Theoretic background”), we find the first three chapters. The literature revue is presented (Chapter 2) divided into two parts: the first concerning the evaluation of the parameters that describe the DDF, and the second concerning the solution of the heat transfer problem. Then, after a brief description of the experimental facility of the laboratory (Chapter 3), we step into the second portion of this document, that is, the modeling approach in which we explain the experimental correlations necessary to evaluate the DDF (Chapter 4) and the

1. Trade Mark of MathWorks

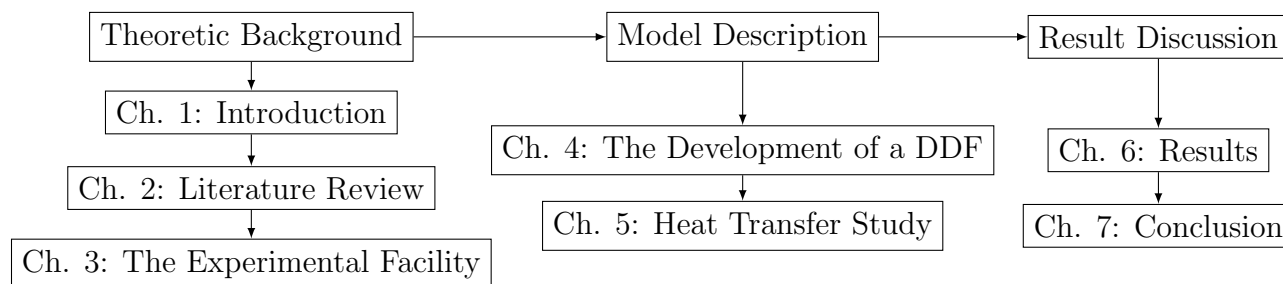


Figure 1.3 Thesis plan

solution of the droplet heat transfer problem (Chapter 5). Finally, in the last part of this document, a comparison between the predictions of the code and the experimental data is presented (Chapter 6), followed by the limitations of our code and the future work necessary to improve the developed program (Chapter 7).

CHAPTER 2

LITERATURE REVIEW

DCHXs are extensively used in numerous power applications: nuclear power stations, cooling towers, petroleum, thermal and chemical plants (Marshall, 1955; Takahashi *et al.*, 2001): for this reason, the complex phenomena happening during the DCHX operation (some of them already explained in Chapter 1) have been studied by many researchers. Nevertheless, it seems that in the scientific literature there is not a complete model capable of correlating these phenomena and the overall thermal power exchanged for a given thermodynamic condition. Since our purpose is to find this correlation, the literature review lists many research works concerning these phenomena. In order to be clear, the literature review is divided into two parts, each of which focuses on the following basic aspects of our research:

- the droplet size evaluation, the atomization process and the development of a statistical function (Section 2.1);
- the heat and mass transfer from liquid droplets in a gaseous environment (Section 2.2).

2.1 Droplet Size Evaluation

Since spray systems find many applications (i.e., air cooling, fire protection, combustion), the need of evaluating their efficiency is justifiable. The most common way to characterize the efficiency is to provide the dimensions of droplets coming from the nozzles. This goal can be reached by using droplet-size analyzers.

There are different types of analyzers and they differ by the method to measure spray droplets. Two main methods are available, imaging and scattering optical methods. The former analyzes the light recorded by a camera while the spray is operating (optical imaging analyzers). Instead, the latter measures the scattered light intensity caused by falling droplets (laser diffraction analyzers or optical array probes). We point out that these methods are non-intrusive, hence the spray behavior is not influenced and the measurements are very accurate (Schick, 2006).

In our thermal facility we do not have any of these devices, so, to evaluate the size of droplets issuing from the spray nozzle, we studied scientific works made by other researchers on this theme. Most of these can be found in combustion research field, since in many ignition chambers, liquid fuel is sprayed through a nozzle. In spite of that, to understand these works, it is necessary to have a clear idea about the fundamental process happening in

nozzle systems, the atomization. Thanks to this process, liquid passes from a continuous to a disperse phase: since this process deeply affects the droplet size, a brief summary about atomization is necessary.

2.1.1 The Atomization Process

Atomization is the conversion of bulk liquid into droplets (Lefebvre, 1989); this process can be reached in several ways (mixing liquid with air, forcing the liquid to pass through an orifice, etc.) depending on the type of nozzle used. Usually, two stages of atomization are defined; the former takes place close to the spray nozzle and is named first atomization. As its name suggests, in the first atomization there is the first formation of liquid droplets. Liquid coming from the nozzle is still in a continuum phase, but it is highly unstable (because of the high relative velocity between liquid and gas) so, the instabilities firstly make the liquid to convert into ligaments and then into droplets, as showed in Figure 2.1 (Crowe, 2005). However, droplets are not yet in a stable condition; as a matter of fact, larger droplets traveling at high velocities are subject to deformations, and if the surface tension is not high enough to hold them, droplets break-up and the secondary atomization takes place (Crowe, 2005).

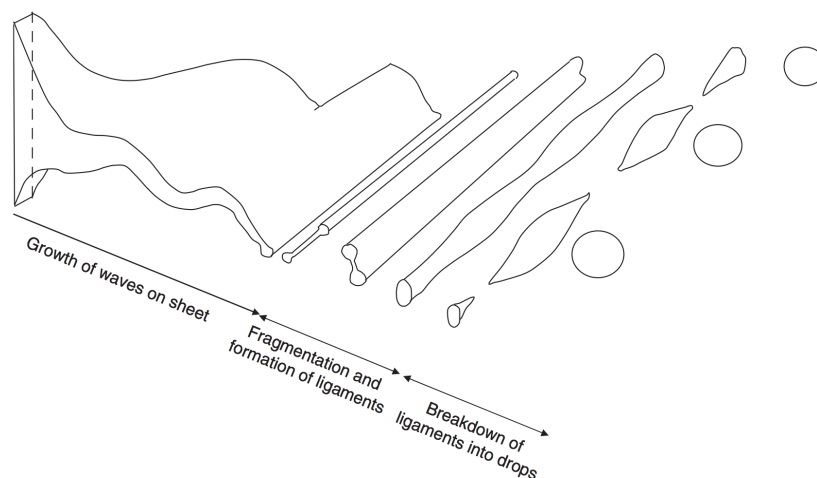


Figure 2.1 Atomization process: formation of ligaments and droplets (adapted from N. Dombrowsky and W. R. Johns, *Chem. Eng. Sci.*, 18, 203–214, 1963)

As it can be easily understood, atomization is difficult to study, since both types depend on geometric characteristics of the nozzle and on thermodynamic conditions of the liquid (Lefebvre, 1989; Schick, 2006). In the scientific literature, it is possible to find several models describing atomization; even if all of them have been collected by Ashgriz (2011) into his

handbook, we did not include any of them in our modeling approach. Instead, we focused our research on the influence that those factor may have on the final droplet size.

The factors affecting the final atomization quality are of different natures: they may refer to the features of the nozzle, as the type of spray (hydraulic, twin-fluid, rotary, ultrasonic or electrostatic nozzle), their size (orifice diameter and axial length), the flow pattern they provide (flat, hollow or full cone) and the cone angle at the nozzle exit. Another factor is the temperature of the sprayed fluid, since it affects the thermodynamic properties (we will see later that the droplet size is a function of these properties, among all viscosity and surface tension). Finally, the working conditions that have to be considered are the liquid flow rate in the nozzle, the temperature and the pressure of the environment in which the fluid is sprayed.

In order to understand how these parameters influences the atomization, the qualitative study made by Schick (2006) can be used. In fact, he has proved that a high atomization quality (droplets with low size), can be reached by increasing the chamber pressure, the liquid temperature (viscosity and surface tension decrease with increasing temperature) and, if it is possible, the spray cone angle; on the other side, an increment in liquid flow rate has the effect of degrading the atomization quality (i.e., big size droplets are expected).

2.1.2 Droplet Distribution Function (DDF)

The latter qualitative analysis is not enough; in fact, it helps to understand how the single factor acts on droplet size, while all of them simultaneously affect the atomization process. For this reason, from the beginning of '80s to the end of '90s, researchers analyzed spray behavior in order to develop experimental correlations linking the aforementioned factors and the droplet size.

This is a complex task because the physical variables affecting the atomization process are numerous and it is not easy to consider all of them in a unique correlation (in fact, the more variables that are considered, the less accurate the correlation becomes). Moreover, it is not easy to define the droplet size: how can we define the *droplet size* when, independently from the working conditions, a spray nozzle always provides a range of drops of different physical dimensions? For these reasons, researchers studied the statistical distributions describing droplet size and developed correlations that evaluate the characteristic diameters of these distributions.

Let us assume $F(D)$ (i.e., DDF) to be the cumulative probability of having droplets with diameter lower than D ; the aforementioned correlations can estimate (Lefebvre, 1989):

- $D_{0.1}$, the diameter that gives 0.1 when used in the cumulative distribution $F(D)$;

- D_{peak} , the diameter corresponding to the peak of the $F(D)$ curve;
- $D_{0.5}$, which is the mass median diameter of $F(D)$;
- $D_{0.632}$, the diameter that gives 0.632 when used in the cumulative distribution $F(D)$;
- $D_{0.999}$, the maximum droplet diameter predicted by $F(D)$;
- D_{32} , or *SMD*, the Sauter mean diameter, defined as

$$D_{32} = \frac{\sum_{i=1}^N n_i D_i^3}{\sum_{i=1}^N n_i D_i^2} \quad (2.1)$$

Unlike other parameters, the Sauter mean diameter (Equation 2.1) has not a statistical meaning; instead, it represents the ratio between the total volume occupied by droplets and the total surface area.

In the scientific literature, several correlations are available and these have been collected by Ashgriz (2011); among others, Lefebvre (1989) developed a considerable number of these experimental correlations which are still used today (Semiao *et al.*, 1996).

Nevertheless, the knowledge of the statistical diameters is not enough and $F(D)$ (i.e., DDF) has to be found. Ashgriz (2011) collected the available methods to estimate droplet size distributions; some of them are complex, as the use of the Maximum Entropy Formalism, others are easier, as the use of empirical distributions. One of the first distributions on this topic has been proposed by Rosin and Rammler (1933), who used the Weibull distribution to describe coal-particle sizes. This law is still used because of its simplicity. In spite of that, other statistical functions are available, such as the normal and the log-normal, the upper-limit, the root-normal and the Nukiyama-Tanasawa distribution (Lefebvre, 1989; González-Tello *et al.*, 2008; Ashgriz, 2011); these laws require experimental observations to find the parameters describing those distributions.

Once the characteristic diameters are defined and a statistical distribution for droplet size is chosen, it is possible to use closure equations to find the DDF for given working conditions (i.e., liquid temperature, flow rate, chamber pressure, etc.). For instance, Zhao *et al.* (1986) developed the closure equations for a Rosin-Rammler distribution and the characteristic diameters.

From a broader prospective, the elements necessary to evaluate a DDF have been presented. In fact, the use of experimental correlations allows the evaluation of one, or more, statistical laws. In spite of that, two weak points must be highlighted:

1. The use of these correlations is not always straightforward. In fact, despite the extensive literature on this topic, their use should be limited to applications where the working

conditions are similar to the laboratory conditions in which these correlations were developed. As it can be easily understood, it is hard to respect this constraint.

2. The statistical approach presented here does not take into consideration two phenomena pertaining to the dynamics of liquid droplets. The first one has been already mentioned, it concerns the secondary atomization: as said before, bigger droplets are subject to break-up (this phenomenon obviously affects the real statistic distribution). The second concerns the mutual interaction of liquid droplets. In fact, it may happen that two (or more) droplets collide to form a bigger droplet, or a large number of relatively smaller droplets. Despite the complexity of droplet break-up and collision, in scientific literature models describing these two phenomena are available (Crowe, 2005; Beck and Watkins, 2002; Ashgriz, 2011).

For these reasons, the use of empirical correlations to find the DDF is questionable. That being said, the DDF obtained by following this approach is valid only at a first approximation and can be far from the actual distribution; this aspect will be discussed through the course of this thesis.

2.2 Heat and Mass Transfer from Liquid Droplets

The second important problematic studied in this work is the heat and mass transfer from liquid droplets. Some of the questions concerning this topic have already been presented in Chapter 1; here we provide a more detailed explication on this problem and some possible solutions found in the scientific literature. In particular, our research focuses on two main heat transfer modes: convection and phase change (i.e., evaporation).

Convection from liquid droplets in a gaseous environment is not easy to understand because phenomena such as the liquid circulation inside droplets (Celata *et al.*, 1991) or droplet deformation (Ashgriz, 2011; Crowe, 2005) affect the convection and can be difficult to predict. For these reasons, it is common to find in the literature the hypothesis of considering liquid droplets as solid spheres. These approximations help to simplify the problem in order to evaluate the energy and mass exchanges. Moreover, it has been proven that these assumptions do not lead to significantly high errors (Celata *et al.*, 1991).

One of the most detailed works on this topic has been presented by Sripada *et al.* (1996) and Huang *et al.* (1996). These authors developed a model by writing the conservation equations in spherical coordinates for falling water droplets in a steam environment (i.e., cylindrical control volume). Also, based on their modeling approach, Sripada *et al.* (1996) and Huang *et al.* (1996) added the effect of steam condensation on spray droplets (considered as solid spheres). Sripada *et al.* presented the conservation equations (mass, momentum and

energy), the corresponding boundary conditions and some assumptions (such as Re number of the order of 100, uniformly spaced droplets in the control volume) necessary to solve the problem. Instead, Huang *et al.* (1996) analyzed the results obtained by Sripada *et al.* and, consequently, estimated the behavior of key physical properties, i.e., surface tangential velocity ($u_{g,\theta}|_{r=1}$), condensation velocity ($u_{g,r}|_{r=1}$), Nusselt (Nu) and Sherwood (Sh) numbers and surface shear stress (τ), as a function of time, droplet angular position and radius. For instance, they showed that Nu (and Sh , using the Reynolds analogy) and $u_{g,r}|_{r=1}$ reach the highest value on the stagnation point, no matter the considered time.

Since Sripada *et al.* (1996) and Huang *et al.* (1996) solved the two dimension conservation equations in spherical coordinates, the solution is a function of the time t , the radius r and the polar angle θ . If we neglect the dependence on θ and we limit our study only on r and t , the solution becomes easier to find. For instance, let us assume that we want to find the temperature variation of a free-falling liquid droplet T ; then, the heat conduction equation to be solved is

$$\frac{\partial^2 T}{\partial r^2} + \frac{2}{r} \frac{\partial T}{\partial r} = \frac{1}{\alpha} \frac{\partial T}{\partial t} \quad (2.2)$$

where α is the thermal diffusivity of the liquid droplet. Depending on the boundary conditions, the solution of this problem can be found using the method of separation of variables, a topic well analyzed in Carslaw (1959) and in Ozisik (1993), or even much more easily with the lumped capacitance method, whenever it is applicable (Incropera *et al.*, 2007).

Celata *et al.* (1991) solved the previous differential equation in order to study the behavior of droplet temperature established in a condensing steam environment. As initial conditions, they assumed the droplets at sub-cooled liquid condition and the vapor at saturation. Assuming conduction heat transfer inside the droplet, Celata *et al.* (1991) have calculated the spray-droplet mean temperature by averaging the solution on the radial coordinate. That is, the mean temperature is only a function of time. Furthermore, to take into account the effect of liquid circulation inside the droplet, they introduced a coefficient as a function of Péclet number, which permitted a better agreement of model predictions with experimental data to be achieved. Takahashi *et al.* (2001) have compared the predictions of Celata *et al.* model with their own experimental data. Thus, they were able to show that the model was not adequate to evaluate the liquid temperature for non-dimensional distances lower than 6 (the non-dimensional distance is defined as $\mathbf{X} = x/D$, where x is the distance from the nozzle and D is the droplet diameter).

The second main phenomenon, the phase change, is not any less easier to study. Sripada, Huang and Celata imposed steam condensation as a boundary condition, but elsewhere researchers studied droplet evaporation, phenomenon occurring in air-cooling systems. A detailed work on this aspect has been presented by Marshall (1955), who studied the heat and

mass transfer from a liquid spray to air during air-drying processes by including the effect of the size of droplets. In order to do that, Marshall used the Rosin-Rammler equation. In his modeling approach, he applied the energy balance to liquid droplets, supposing the droplet evaporation rate equates to the convection heat transfer rate. From this, he was able to calculate the mass evaporation rate. Moreover, Marshall (1955) used a correlation for the Nusselt number (Nu) as a function of the Reynolds (Re) and Prandtl (Pr) numbers; using the Reynolds analogy, the correlation links the Sherwood number (Sh) with Reynolds and Schmidt (Sc). This correlation, proposed in a previous work (Ranz and Marshall, 1952), is necessary to estimate the convective heat and the mass transfer coefficients.

As it can be understood, the phase change problem is not easy to handle. In fact, since in DCHXs there is a mutual contact between liquid and steam, it is hard to predict if liquid evaporation will predominate on steam condensation. Furthermore, the scientific literature is not helpful: first of all, we have works that impose steam condensation on liquid droplets (Sripada *et al.*, 1996; Huang *et al.*, 1996; Celata *et al.*, 1991; Takahashi *et al.*, 2001). On the other hand, we must face the fact that the working conditions in our DCHX may allow liquid evaporation instead of steam condensation, as it happens in air-cooling system (Marshall, 1955). We opted for studying liquid evaporation. However, the question is still open and not yet solved.

CHAPTER 3

THE EXPERIMENTAL FACILITY

Before describing the modeling approach, it is necessary to present the experimental setup in the “Altan Tapucu” Thermo-Hydraulic laboratory. It consists in two coupled thermal loops; one working at pressures lower than 40 *bar* and one working at pressures ranging from 220 to 240 *bar*. Note that these two loops will not be described in detail, however, their description can be found in Muftuoglu and Teyssedou (2013).

After a brief but necessary explanation of its operation (Section 3.1), we present in a more detailed way two components of the thermal loop, the test section (Section 3.2) and the quenching chamber (Section 3.3). The former is the key element of the whole facility, since choked flow conditions occur here. However, steam coming from the test section is at a high temperature, so a heat exchanger (i.e., DCHX) is needed in order to cool down the steam. Since our aim is to analyze the heat transfer in the DCHX, a description of the quenching chamber shown in Figure 3.1 is required.

3.1 The Super Critical Water Loop (SCWL)

The main purpose of the steam-water loop is to study super-critical steam choked flow (Muftuoglu and Teyssedou, 2013). In order to reach this fluid-dynamic condition, a large pressure drop is needed. In fact, coupling two thermal loops working at different pressures can satisfy this constraint. As already mentioned, two loops are present, one working with pressure lower than 40 *bar*, while the other can support pressures between 220 and 240 *bar* (super-critical water pressure). In spite of this, to understand the experimental facility operation, it is not necessary to describe the low pressure water loop in detail, but it is sufficient to focus on the Super Critical Water Loop (SCWL) shown in Figure 3.1.

Let us analyze the flow diagram given in this figure: the isolation valve identified with “V-1” acts as the first conjunction between the two loops; in fact, water coming from the low pressure loop enters into the SCWL through this valve. This means that the water has a low pressure ($p_{H_2O} < 40 \text{ bar}$) and a temperature close to saturation. Since these conditions are too high and they may affect the operation of certain components in the thermal loop, a heat exchanger (“Cooler” technical designation in Figure 3.1) is needed to cool the water down. Moreover, since solid particles dispersed in the water degree may affect the operation of other components, a filter (“Filter”) is installed next to the cooler. Thanks to the cooler and the

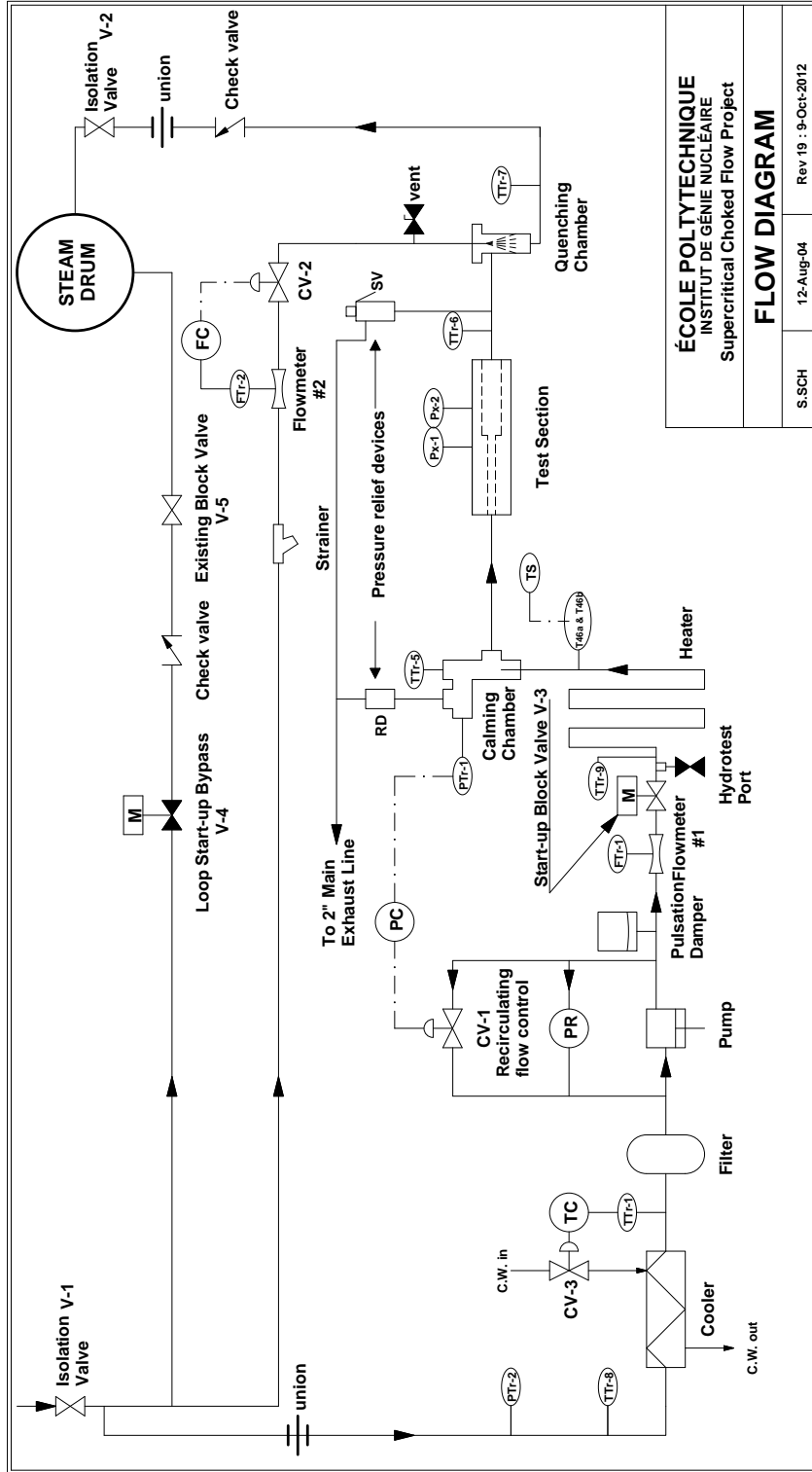


Figure 3.1 Flow Diagram

filter, the subsequent water loop elements can safely work. One of the key equipment is a six pistons variable-speed pump, in which the maximum allowable inlet water temperature is $65^{\circ}C$. Since the water must reach the super-critical pressure, the pressure drop in the pump can be higher than 200 *bar*. To avoid any fluctuation in water pressure due to the six pistons, a damper is installed next to the pump. This component can be seen as a chamber containing nitrogen at high pressure ($p_{N_2} = 206.8 \text{ bar}$): the nitrogen and the water never come into contact, because they are separated by a natural rubber membrane. In order to reach super-critical conditions, thermal power is needed in such a way to increase the water temperature. This task is performed by the “Heater” (Figure 3.1), that consists of a 11.2-*m*-long tube where water at high pressure ($p_{H_2O} > 220 \text{ bar}$) flows. The heater can transfer to the water a power of up to 550 *kW* via a difference in electric potential of 110 *V* and an electrical current of 5000 *A*.

At the outlet of the heater, water has reached super-critical conditions ($p_{cr} > 220.6 \text{ bar}$, $T_{cr} > 373.9^{\circ}C$), however, the flow coming from the heater can be highly unstable because at the critical point the thermodynamic properties change abruptly in a short period of time (for instance, the density becomes 800 times lower). To avoid instabilities due to super-critical water stratification, the “Calming Chamber” (Figure 3.1) is used. Then, super-critical water in a stable condition enters into the test section where choked flow condition occurs. In the “Test Section” (Figure 3.1) the pressure decreases, so we can say that this component acts as the second conjunction between the two loops. In spite of the pressure reduction, steam temperature is still too high, thus it must be cooled down in the “Quenching Chamber” (Figure 3.1) where mixing between steam and water coming from the isolation valve “V-1” takes place. A more detailed description of the test section and the quenching chamber is given in the following sections.

3.2 The Test Section

Before presenting the test section, it is necessary to characterize the water flow present in this component. As aforementioned, the super-critical water reaches choked flow conditions in the test section; a brief explanation on this fluid dynamic condition is necessary in order to understand the geometric characteristics of our test section.

When a fluid flows from a high-pressure to a low-pressure environment through a choke, its velocity increases, thus, causing an increase in fluid velocity proportional to the pressure differential between the two environments. This is generally true until the pressure ratio

reaches a critical value, defined as (isoentropic transformation)

$$\frac{p_{out}}{p_{in}} = \left(\frac{2}{\gamma + 1} \right)^{\frac{\gamma}{\gamma - 1}} \quad (3.1)$$

where γ is the ratio of specific heats. In fact, if the pressure ratio is higher than the critical one, the fluid velocity becomes sonic, giving rise to a choked (or critical) flow. At these conditions, any increase in upstream pressure (or decrease in downstream pressure) does not affect the flow velocity, which is constant (hence, the name of *choked flow*). This means that if the velocity does not increase anymore, at first approximation (neglecting any change in fluid density), the mass flux becomes independent of the pressure ratio and is consequently constant (Muftuoglu and Teyssedou, 2013).

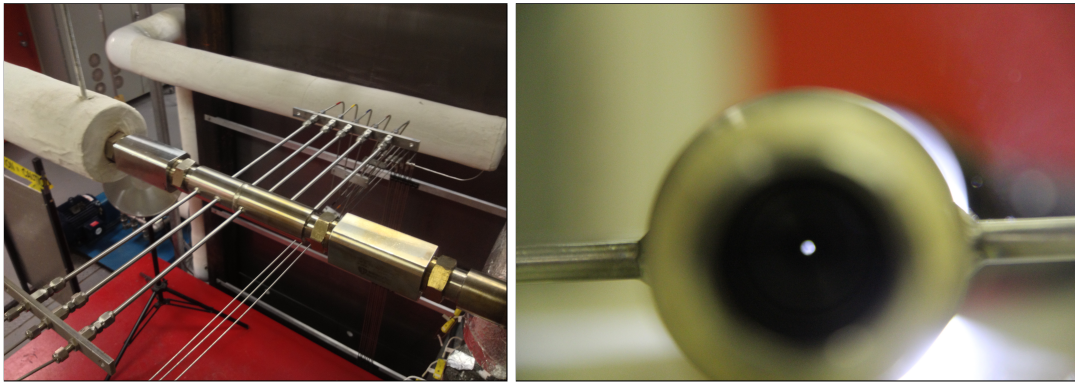


Figure 3.2 Test section

As already mentioned, the test section used in the laboratory has been designed in order to study super-critical water choked flow; Figure 3.2 shows two views of this key component. It is a tube manufactured from a solid Hastelloy C-276 cylinder equipped with eight pressure taps (three upstream and five downstream). On the left side of Figure 3.2 we can see how the test section is installed in the loop, while on the right hand side of the same figure, we highlight the orifice plate located inside into this component. In order to be more clear, Figure 3.3 shows the schematics of the test section; in fact, when steam enters into this element, at the beginning it flows in a 4-*mm*-diameter channel (here the pressure is super-critical). Afterwards, it is forced to pass through a restriction of 1 *mm* in diameter and 3.17 *mm* in length and finally it discharges into a 23.7-*mm*-diameter channel, where the pressure decreases rapidly.

It is difficult to define, from a thermodynamic standpoint, the flow evolution taking place in the test section (Muftuoglu and Teyssedou, 2013). The orifice plate shown in Figure 3.3

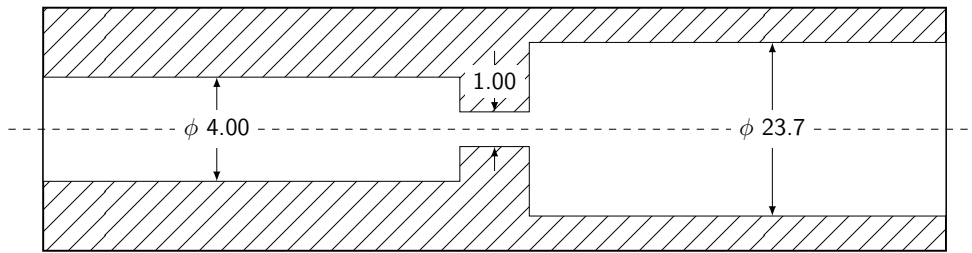


Figure 3.3 Test section scheme

is not a valve which means the transformation is not necessary isenthalpic. Obviously, it cannot be considered isentropic as well. Experimental data shows that the flow evolution along the discharge lies between the isenthalpic and the isentropic line (for more details, see Section 5.1). Nevertheless, steam leaving from the test section has a temperature that can be too high and for the maximal design value of the low pressure loop (i.e., 250°C) it is cooled down in the quenching chamber.

3.3 The Quenching Chamber

The task of cooling steam coming from the test section is performed in the quenching chamber (DCHX). Here, super heated steam mixes with sub-cooled water coming from the valve “V-1” in Figure 3.1 (in fact, steam and water have the same pressure). The direct

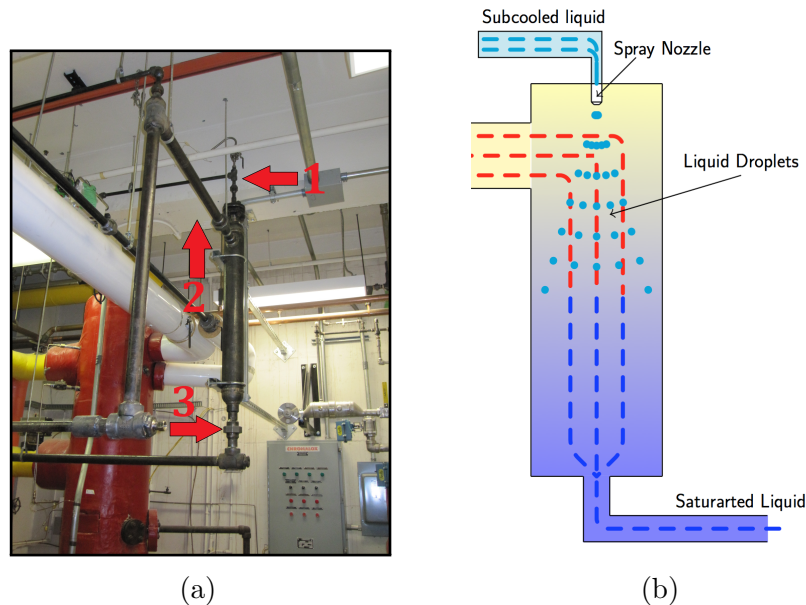



Figure 3.4 (a) Photo of the quenching chamber (b) scheme of the quenching chamber

contact between hot and cool fluid takes place in the quenching chamber, that is a pipe (Def. 4”SCH-80-PIPE-CAP) for which dimensions are 0.9144 *m* (3 *feet*) in length and 0.1143 *m* (4.5*inches*) in diameter. These dimensions allow the pipe to work with pressures lower than 40 *bar* (Cascella and Teyssedou, 2013). The left hand side of Figure 3.4 shows a picture of the quenching chamber before adding the thermal insulation. Sub-cooled water enters into the heat exchanger through the duct “1”, while steam enters through the duct “2”. Thereafter, a mixture of steam and liquid exits from duct “3” and is finally sent to the “Steam Drum” as shown in Figure 3.1. The right hand side of Figure 3.4 shows a scheme of the DCHX. Particularly, in this figure we highlight the presence of a spray nozzle in the quenching chamber (hidden component in the photo). This component, placed at 4 *cm* below the top of the pipe, sprays water inside the vessel under the form of tiny droplets, maximizing the contact surface area and, in turn, the heat transfer.



PERFORMANCE DATA

D *At the stated pressure in bar.

Body Inlet Conn. (in.)	Orifice Disc No. – Core No.	Orifice Dia. Nom. (mm)	Capacity (liters per minute)*										Spray Angle (°)*		
			0.7	1.5	2	3	4	6	7	10	15	20	1.5	3	6
1/4	D1-31	.79	.31	.41	.49	.59	.67	.80	.92	1.0	1.2	1.4	49	47	43
	D1.5-31	.91	.39	.51	.63	.76	.86	1.0	1.2	1.3	1.6	1.8	57	65	53
	D2-31	1.0	.45	.59	.72	.86	.98	1.2	1.4	1.5	1.8	2.0	62	63	61
	D3-31	1.2	.49	.64	.80	.95	1.1	1.3	1.5	1.6	1.9	2.2	63	65	63
	D1-33	.79	.32	.42	.46	.56	.64	.78	.90	.98	1.2	1.4	27	32	35
	D1.5-33	.91	.42	.55	.63	.75	.85	1.0	1.2	1.3	1.6	1.9	37	43	45
	D2-33	1.0	.47	.62	.78	.95	1.1	1.3	1.5	1.7	2.0	2.3	45	52	55
	D3-33	1.2	.57	.75	.95	1.1	1.3	1.6	1.8	2.0	2.5	2.8	48	54	57
	D4-33	1.6	.78	1.0	1.3	1.5	1.7	2.1	2.4	2.7	3.3	3.7	50	56	61
	D1-35	.79	.30	.39	.48	.58	.65	.78	.90	.97	1.2	1.3	19	23	26
	D1.5-35	.91	.41	.54	.63	.76	.85	1.0	1.2	1.3	1.5	1.7	23	27	29
	D2-35	1.0	.53	.70	.83	.99	1.1	1.3	1.5	1.7	2.0	2.2	40	44	47
	D3-35	1.2	.58	.76	.98	1.2	1.3	1.6	1.8	2.0	2.4	2.8	45	50	52
	D4-35	1.6	1.0	1.3	1.6	2.0	2.3	2.8	3.2	3.5	4.2	4.8	68	70	71
	D5-35	2.0	1.3	1.7	2.2	2.6	3.0	3.6	4.1	4.5	5.5	6.3	67	69	71
	D2-56	1.0	–	–	.80	.98	1.1	1.4	1.6	1.8	2.2	2.5	–	14	17
	D3-56	1.2	–	–	1.1	1.3	1.6	1.9	2.2	2.4	3.0	3.4	–	20	23
	D4-56	1.6	–	1.3	1.8	2.2	2.5	3.1	3.6	4.0	4.8	5.6	20	26	29
	D5-56	2.0	1.4	1.8	2.5	3.0	3.5	4.3	4.9	5.5	6.7	7.8	26	32	34
	D6-56	2.4	2.2	2.8	3.7	4.5	5.3	6.5	7.5	8.5	10.2	11.9	34	39	41
D7-56	2.8	2.9	3.8	4.9	6.0	6.9	8.5	9.8	11.0	13.5	15.6	45	52	54	
D8-56	3.2	3.7	4.9	6.2	7.6	8.8	10.8	12.4	13.9	17.0	19.6	52	57	59	
D10-56	4.0	5.1	6.7	8.6	10.6	12.2	15.0	17.3	19.3	24	27	62	65	67	

Figure 3.5 Spray System catalogue

The spray nozzle is manufactured by Spray Systems¹. This component is manufactured in stainless steel and belongs to the UniJet family. Moreover, the Spray System catalog (Figure

1. Trade Mark of Spray Systems

3.5) puts our nozzle under the Type *D*, which means “Full Cone Spray Nozzle, Disc and Cone Type”. As the name says, this nozzle provides a full cone pattern (left side of Figure 3.6) and the assembly includes six elements (right side of Figure 3.6): a female and a male body, which form the nozzle body, a slotted strainer, a core, a disc and finally a tip retainer.

In the Spray System catalog, the nozzle body codes are $\frac{1}{4}$ TD4-56 for the female body and $\frac{1}{4}$ TTD4-56 for the male one, which characterize the working conditions. For instance, they affect the choice of the disc and core, leading to a disc orifice diameter of 1.6 *mm* (0.063”). Moreover, using these nozzle components, the maximum allowable flow rate and spray angle become functions of the discharge pressure through the nozzle. In the present case, we have a discharge pressure of 2.76 *bar* and, accordingly, a maximum flow rate of 0.035 *l/s* and a spray angle of 26°.

We must point out that this information is needed, because the aforementioned parameters have a strong influence on the atomization process. Furthermore, as it will be seen in Chapter 4, the dimensions of sprayed droplets have to be known to evaluate DCHX performances, however, the manufacturer’s catalog does not provide this information; it is limited to a note which says “a finely atomized uniform spray pattern” is provided. This lack of information related to the droplet size made the task of evaluating quenching chamber behavior quite difficult. Therefore, the information available in the catalog has been used in order to estimate the droplet size, and consequently to build one of the basis of the model as it will be seen in the next chapter.

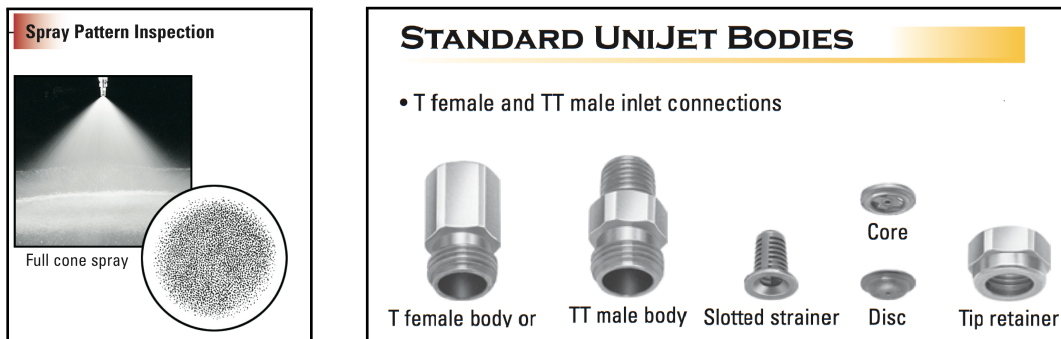


Figure 3.6 Spray nozzle components and flow pattern (Spray System Catalog)

CHAPTER 4

DEVELOPMENT OF A STATISTIC DISTRIBUTION FUNCTION FOR THE DROPLET SIZE

The droplet size is a fundamental parameter that affects the droplet-velocity field and, in turn, the heat transfer. However, as previously mentioned, the droplet size depends on a large set of independent variables, such as the geometrical characteristics of the nozzle and the thermodynamic conditions of the cooling liquid (Section 4.2).

Here we present the methodology to evaluate a statistical distribution function for the droplet size: we present the Sauter mean diameter (already defined in Equation 2.1), its meaning (Section 4.1) and how to calculate it with experimental correlations (Section 4.1.1). Afterwards, we collect the different DDFs available in literature (Section 4.2), focusing on the Rosin-Rammler distribution function (Section 4.2.1).

4.1 The Sauter Mean Diameter

The topic of the droplet size evaluation has been studied by many in depth researchers because this parameter affects the spray system efficiency. In spite of that, it is not easy to define the droplet size when a nozzle sprays droplets of various diameters; one could evaluate the DDF by directly measuring the droplet dimensions (if it is possible) or by using empirical correlations. Moreover, for the latter, it is necessary to define characteristic diameters that describe the DDF; hence, these are:

- $D_{0.1}$, the diameter that gives 0.1 when used in the cumulative distribution $F(D)$;
- D_{peak} , the diameter corresponding to the peak of $F(D)$ curve;
- $D_{0.5}$, which is the mass median diameter of $F(D)$;
- $D_{0.632}$, the diameter that gives 0.632 when used in the cumulative distribution $F(D)$;
- $D_{0.999}$, the maximum droplet diameter predicted by $F(D)$;
- D_{32} , or *SMD*, the Sauter mean diameter.

In order to better understand the meaning of these characteristic values, Figure 4.1 shows their location on a given DDF. Probably the most used of these characteristic values is the Sauter mean diameter (SMD or D_{32}), defined as:

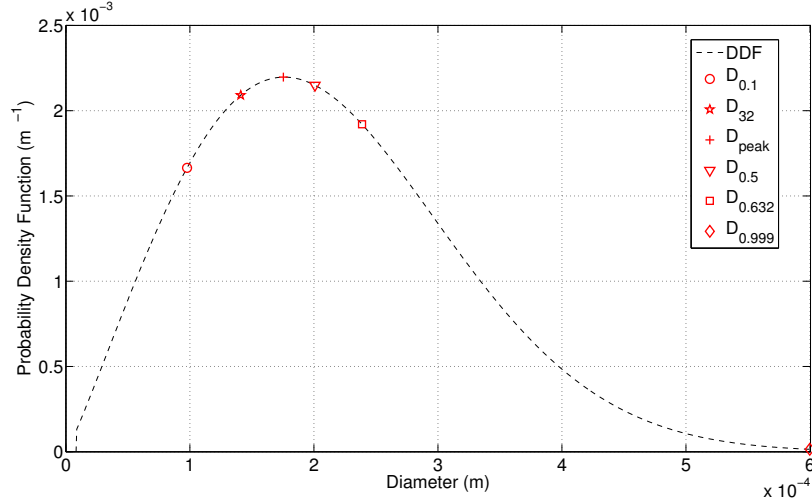


Figure 4.1 Location of the characteristic diameters on a given DDF

$$D_{32} = \frac{\sum_{i=1}^N n_i D_i^3}{\sum_{i=1}^N n_i D_i^2} \quad (4.1)$$

where N is the total number of droplets and n_i is the number of droplet with diameter D_i . The reason for its common use in this research field lies in its meaning; Lefebvre (1989) defines D_{32} as “the diameter of the drop whose ratio of volume to surface area is the same as that of the entire spray”.

Because of its importance, researchers analyzed D_{32} for different spray nozzles, in order to find a relationship between the nozzle working conditions and the Sauter mean diameter. Doing so is not an easy task since a satisfactory correlation should take into account differ-

Table 4.1 Experimental correlations available in scientific literature

Correlation	Application	Source
$D_{32} = \frac{3}{\frac{1}{i} + \frac{C_{2L}}{4\sigma} \left[U_a^2 \left(\frac{\dot{m}_A}{\dot{m}_L} \right) + U_l^2 \right]}$	Pre-filming air-blast nozzles	Barreras and Eduardo (2006)
$D_{32} = Ad_0^{0.12} d_{in}^{0.56} \frac{\mu_L^{0.12}}{\mu_A} \left(\frac{\dot{m}_L}{\dot{m}_A} \right)^{0.3}$	Plain jet air-blast nozzles	Broniarz-Press <i>et al.</i> (2009)
$D_{32} = 64.73d_0 Re \left(\frac{L}{d_0} \right) - 0.014d_0 We^{0.533}$	Plain orifice nozzles	Cleary <i>et al.</i> (2007)
$D_{32} = 2.25\sigma^{0.25} \mu_L^{0.25} \dot{m}_L^{0.25} \Delta P^{-0.5} \rho_A^{0.25}$	Swirl nozzles	Lefebvre (1989)

ent parameters, i.e., the geometrical characteristic of the nozzle (spray cone angle, length of the initial liquid sheet), the ambient pressure, the thermodynamic conditions of the liquid (Lefebvre, 1989; Schick, 2006). In addition, the more parameters are considered, the less the correlation is accurate (Ashgriz, 2011). Nowadays, many experimental correlations are available in literature (Table 4.1 shows some of them). Ashgriz (2011) collected many relationships encountered in industrial applications into his handbook, which simplifies the complex task of choosing the suitable correlation for our case. In particular, since the spray nozzle falls into the swirl and plain orifice categories, we focus our attention on four correlations provided into recent Ashgriz's handbook:

$$D_{32} = 52\dot{m}_L \Delta P^{-0.397} \nu^{0.204} \quad (4.2)$$

$$D_{32} = 64.73 d_0 Re \left(\frac{L}{d_0} \right) - 0.014 d_0 We^{0.533} \quad (4.3)$$

$$D_{32} = 2.25 \sigma^{0.25} \mu_L^{0.25} \dot{m}_L^{0.25} \Delta P^{-0.5} \rho_A^{0.25} \quad (4.4)$$

$$D_{32} = 4.52 \left(\frac{\sigma \mu_l^2}{\rho_v \Delta P_l^2} \right)^{0.25} (t \cos \theta)^{0.25} + 0.39 \left(\frac{\sigma \rho_l}{\rho_v \Delta P_l} \right)^{0.25} (t \cos \theta)^{0.75} \quad (4.5)$$

Equation 4.2 has been developed by Orzechowski (1976), Equation 4.3 has been developed by Cleary *et al.* (2007) and Equation 4.4 and 4.5 has been developed by Lefebvre (1989).

The reason why we chose these equations is because all of them have been developed using water as the working liquid. In fact, since most of the research done in this field is available in combustion literature, the major part of these correlations has been developed using liquid fuel (i.e., kerosene, glycerin) instead of water. It is well known that the thermodynamic properties of fuels are greatly different from water. In particular, liquid fuels have a surface tension smaller than that of water. Thus, using a correlation developed for liquid fuels leads to an underestimation of droplet size of about one order of magnitude.

The use of the aforementioned correlations is not straightforward. Equation 4.2 has not been used because it was impossible to analyze the working conditions in which this correlation has been developed since the reference is in Polish (Orzechowski, 1976). Equation 4.3 (Cleary *et al.*, 2007) has been developed using a nozzle that provides a full cone pattern, however, when increasing the pressure, it predicts an increment of droplet size, and is in disagreement with most of the works done in this field. Equations 4.4 and 4.5, developed by Lefebvre (1989), seem to be valid but Equation 4.4 was found seven years before Equation 4.5. Consequently, in our work we used Equation 4.5 to estimate D_{32} .

We point out that the use of Equation 4.5 is still questionable. In fact, Lefebvre (1989) used six spray nozzles very different from ours. Also, he used nozzles that provided a hollow

cone flow pattern as the cone angle varied between 60° and 90° , while in our case we have a full cone pattern and the spray cone angle is 26° . So, predictions using Equation 4.5 may be far from the real droplet size. Nevertheless, the correlation is based on theoretical aspects of the atomization process that are valid for every nozzle (see Appendix A). In effect, we think that this correlation is always valid so long as we change the two constants present in Equation 4.5 (4.52 and 0.39) which come from Lefebvre's experiments. However, since we did not have the instrumentation needed to evaluate the droplet size (Schick, 2006), we did not change the value of the constants in front of the two terms and we used Equation 4.5 as it has been presented by Lefebvre (1989).

4.1.1 Lefebvre's Correlation (1989)

Several correlations are available in the open literature that allow D_{32} to be determined. We introduced Equation 4.5 in our modeling approach to evaluate the Sauter mean diameter. In this equation σ is the surface tension [N/m], μ_l is the dynamic viscosity of the liquid [Ns/m^2], ρ_l and ρ_v are the density of the liquid and the steam respectively [kg/m^3], ΔP_l is the pressure difference in the nozzle chamber [Pa], t is the sheet film-thickness outside of the discharge orifice [m] and θ is half the spray cone angle. The sheet film-thickness is calculated as (Lefebvre, 1989):

$$t = 2.7 \left[\frac{d_0 FN \mu_l}{(\rho_l \Delta P_l)^{0.5}} \right]^{0.2} \quad (4.6)$$

where d_0 is the discharge orifice diameter and FN is the flow number defined as:

$$FN = \frac{\dot{m}_l}{(\rho_l \Delta P_l)^{0.5}} \quad (4.7)$$

with \dot{m}_l defined as the liquid flow rate [kg/s]. More details on this correlation are listed in Appendix A.

Equation 4.5 shows that D_{32} depends both on the thermodynamic properties and on the geometric characteristics of the spray nozzle. Since the geometric characteristics are fixed and the thermodynamic working conditions are variable, we present in Figure 4.2 the influence of the pressure and the volumetric flow rate on D_{32} . As it can be seen from this figure, D_{32} increases when increasing the liquid flow rate and decreasing the quenching chamber pressure; this result is in agreement with the results presented by Schick (2006). However, when the effect of the pressure is compared to that of the liquid flow rate, the former seems to have a more remarkable influence on D_{32} .

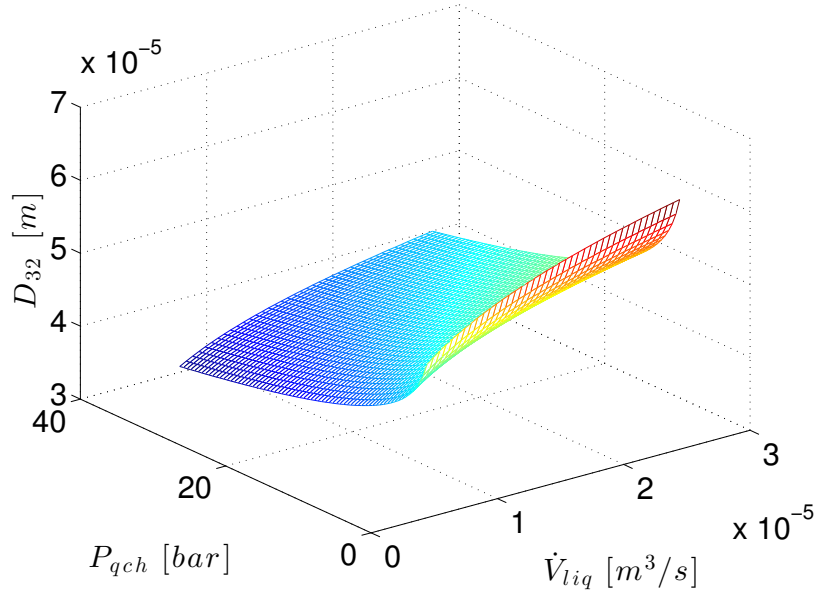


Figure 4.2 D_{32} as a function of P_{qch} and \dot{V}_{liq}

4.2 The Droplet Distribution Function

Characteristic diameters provide a general idea about the droplet size but these should be used to evaluate the actual DDF (Figure 4.1). For this reason, several statistical laws have been studied in order to find the one that best describes the droplet size. These laws are listed by Lefebvre (1989) and Ashgriz (2011):

$$f(D) = \frac{1}{D \ln \sigma \sqrt{2\pi}} \exp \left\{ -\frac{1}{2} \left[\frac{\ln D/\bar{D}}{\ln \sigma} \right]^2 \right\} \quad (4.8)$$

$$f(D) = \frac{\delta D_{max}}{\sqrt{\pi} D (D_{max} - D)} \exp \left\{ -\delta^2 \ln \left[\frac{aD}{(D_{max} - D)} \right]^2 \right\} \quad (4.9)$$

$$f(D) = \frac{1}{2\sigma\sqrt{2\pi D}} \exp \left\{ -\frac{1}{2} \left[\frac{\sqrt{D} - \sqrt{\bar{D}}}{\sigma} \right]^2 \right\} \quad (4.10)$$

$$f(D) = aD^p \exp(-bD^q) \quad (4.11)$$

$$F(D) = 1 - \exp \left[- \left(\frac{D}{D_{0.632}} \right)^q \right] \quad (4.12)$$

In the equations listed above, f represents the probability density function, while F is the cumulative density function. Moreover, D is the droplet diameter, \bar{D} is the mean diameter,

σ is the distribution width and D_{max} is the maximal allowable diameter. In Equation 4.9, the parameters a and δ are defined as follows:

$$a = \frac{D_{max}}{\bar{D}}, \quad \delta = \frac{1}{\sqrt{2 \ln \sigma}} \quad (4.13)$$

The *log-normal* (Equation 4.8), the *upper-limit* (Equation 4.9) and the *root-normal* (Equation 4.10) distributions depend on only two parameters, which are \bar{D} (*log-normal* and *root-normal*) or D_{max} (*upper-limit*) and σ . We point out that D_{max} , \bar{D} and σ require a direct measure of the droplets size during spraying process (unreachable in our case), which makes it difficult to evaluate these quantities. In addition, it is even more difficult to use the Nukiyama-Tanasawa distribution (Equation 4.11), even if it is reliable (Ashgriz, 2011), because it depends on four parameters. Finally, the Rosin-Rammler equation (Equation 4.12) depends on two experimental parameters (q and $D_{0.632}$). However, because this was the first statistical laws used to describe particle sizes (Rosin and Rammler, 1933), it has been deeply studied and nowadays it is possible to use this law even if experimental data is not available.

4.2.1 The Rosin-Rammler Equation

One of the simplest laws available is the Rosin-Rammler cumulative distribution function, where the probability of having the volume fractions for droplets with diameters smaller than a given D is defined by (Rosin and Rammler, 1933):

$$F(D) = 1 - \exp \left[- \left(\frac{D}{D_{0.632}} \right)^q \right] \quad (4.14)$$

where q is a measure of the distribution width (i.e., skewness of the distribution function). It is apparent that applying Equation 4.14 requires a preliminary computation of $D_{0.632}$ and q , which should come from experimental data. However, studies performed by Lefebvre (1989) have shown that for most types of spray nozzles, the value of q varies between 2 and 2.8. Furthermore, Zhao *et al.* (1986) have demonstrated that $D_{0.632}$ can be determined as a function of Sauter mean diameter (Equation 4.1) and q :

$$\frac{D_{0.632}}{D_{32}} = \Gamma \left[1 - \frac{1}{q} \right] \quad (4.15)$$

where Γ is the gamma function. Hence, choosing a value for q between 2 and 2.8 and using one of the experimental correlations to evaluate D_{32} (i.e., Equation 4.5), it is possible to calculate a statistical distribution for droplet size.

Since Equation 4.14 is a cumulative function, its derivative evaluated for a given D_i is the

probability of finding a droplet within the interval $D < D_i < D + dD$:

$$f(D_i) = \frac{dF(D)}{dD} \Big|_{D=D_i} \geq 0, \quad \int_0^\infty f(D) dD = 1 \quad (4.16)$$

Note that the limits zero and infinity used for the droplet size do not have a physical meaning. Thus, we used the limits provided from Zhao *et al.* (1986) who have shown that the lower and the upper limits of the distribution function can be estimated respectively by:

$$D_{0.1} = D_{0.632}(0.1054)^{1/q} \quad (4.17)$$

$$D_{0.999} = D_{0.632}(6.9077)^{1/q} \quad (4.18)$$

At this point, we have enough information to develop a reliable method to calculate the DDF. As it can be understood, the elements on which it is based are D_{32} and q (Cascella and Teysseidou, 2013).

4.3 Considerations on Statistical Methodology

In order to be more clear, Figure 4.3 summarizes the methodology used to develop the DDF. In this methodology, D_{32} becomes the factor that takes into account the thermodynamic conditions of the liquid and the geometrical characteristics of the nozzle. By choosing a value of q^1 , the use of Equations 4.14, 4.15, 4.17 and 4.18 is straightforward (Cascella and Teysseidou, 2013).

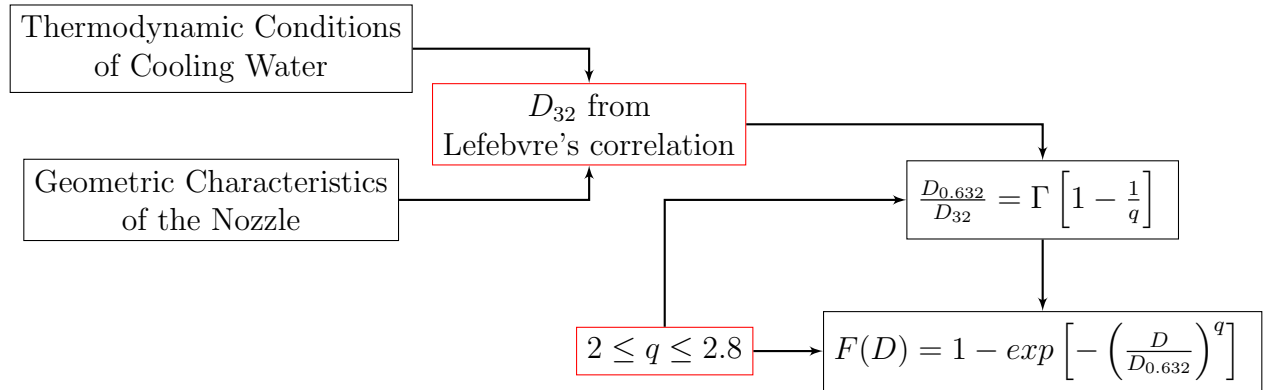


Figure 4.3 Statistical methodology used to evaluate the DDF

To show how the DDF may be affected by D_{32} and q , Figure 4.4 presents four examples

1. The value of q will be chosen later; in fact, in Chapter 6 we will chose this value in order to minimize the difference between predictions and experimental data

of statistical distributions in which the liquid flow rate is kept constant and equal to $2.25 \times 10^{-5} \text{ m}^3/\text{s}$. We evaluated the DDFs for two values of quenching chamber pressures ($P_{qch} = 10 \text{ bar}$ and $P_{qch} = 30 \text{ bar}$) and q ($q = 2.1$ and $q = 2.8$). For each distribution, the liquid temperature is $30 \text{ }^\circ\text{C}$ lower than the saturation temperature ($149.9 \text{ }^\circ\text{C}$ and $200.3 \text{ }^\circ\text{C}$ for $P_{qch} = 10 \text{ bar}$ and $P_{qch} = 30 \text{ bar}$, respectively). We can draw two conclusions from this figure.

The first aspect concerns the influence of the pressure on the DDF; in agreement with Equation 4.5, when pressure increases, the droplet size decreases (see Figure 4.2). This result can be forecasted since an increment in pressure causes an increment in liquid temperature (since it grows with pressure), which causes a decrease in surface tension and, consequently, into a decrease in droplet size.

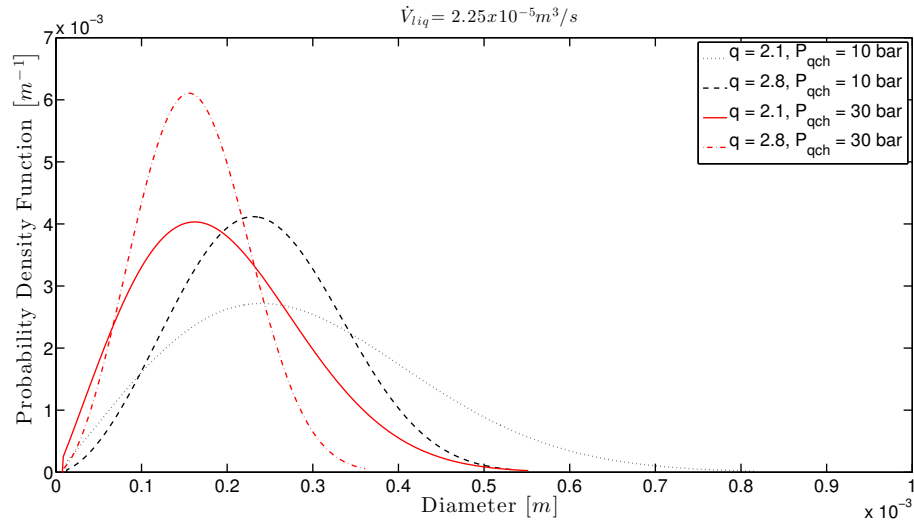


Figure 4.4 Examples of the DDF

Secondly, it is important to underline the effect of q (i.e., skewness); in fact, when q changes, the distribution width significantly changes. From a physical standpoint, this means that for a high value of q , the DDF predicts a spray pattern with uniformly sized droplets. On the other hand, a low value of q makes the DDF predicts a spray pattern having nonuniform droplet sizes.

Limitations of the statistical methodology Finally, it is important to highlight two limitations of the current methodology:

- Because of the lack of instruments able to measure the droplet size (see Section 2.1), the presented methodology has not been completely validated in the laboratory. This means that the method presented here may calculate an incorrect distribution. Also,

we are limited to correctly using Equation 4.5 in order to obtain reliable values for D_{32} . These values have been compared with Schick (2006) and Lefebvre (1989) measurements and were found to be qualitatively in agreement with our data.

- The presented methodology does not take into account the phenomena of droplet collision (i.e., interactions) and droplet break-up. It is clear that these factors affect the DDF but it is hard to integrate them into the proposed model. For this reason, droplet collision and break-up have not been taken into account. Moreover, this hypothesis assumes that the number of droplets in the chamber is low enough. Therefore, the probability of their mutual interaction is very low. Furthermore, their diameter is so small and the velocity of the steam is so low that the surface tension overwhelms any probability of breaking them up.

As it can be seen, there is still work to be done in order to ameliorate the presented methodology, however, we used it to find the droplet size distribution. Because of these limitations, the presented methodology should be considered valid only as a first approximation since it most probably provides a DDF far from the real droplet-size distribution.

CHAPTER 5

HEAT TRANSFER STUDY

The main purpose of this work is to develop a thermodynamic model that best describes the DCHX shown in Figure 3.4. This intent has been reached by analyzing the hardest way possible, since we studied the behavior of every droplet for any given size in a super-critical steam environment. Hence, given the fact that the steam temperature at the test section exit is known (Section 5.1), the solution of the heat transfer problem from sub cooled liquid droplets (considered as spherical) must be found. Two heat exchange modes have been considered, i.e., convection (Section 5.2.1) and evaporation (Section 5.2.2). Then, knowing the heat exchange from droplets, we propose a procedure that links the heat transfer solution with the statistical study in order to find the total thermal power exchanged into the DCHX (Section 5.3).

5.1 The Steam Temperature

In order to study the energy released from the droplets, the parameters that affect the heat transfer must be known. One of these variables is the droplet size which has already studied (Chapter 4) and the other one is the steam temperature.

The evaluation of the latter when entering into the quenching chamber requires a deep knowledge of the thermodynamic transformation occurring in the test section (Figure 3.3), however choked flow conditions are difficult to analyze (Muftuoglu and Teyssedou, 2013). Moreover, at the beginning of this project, the experimental facility was undergoing renovations, and there was not enough available data to completely characterize fluid dynamic conditions. Because of this situation, the evaluation of steam temperature was difficult. Nevertheless, we can still figure out how the transformation will look like. Let us assume water at super-critical conditions at test section inlet, where the thermodynamic conditions are accurately known. If the discharge pressure is also known, it is possible to study two kinds of transformations, i.e., one at constant enthalpy and another at constant entropy. Assuming that the fluid conversion in the test section undergoes one of these two transformations, the steam temperature at test section outlet can be accurately evaluated for these two conditions. However, we do not know if the real transformation is isoenthalpic or isoentropic (Muftuoglu and Teyssedou, 2013), for this reason, we assume that this temperature can be approximated

by the average value calculated as

$$T_2 = \frac{T_{2s} + T_{2h}}{2} \quad (5.1)$$

where T_{2s} is the final temperature of an isentropic expansion and T_{2h} is the final temperature of an isenthalpic one. As an example, let us assume the following water condition at the test section inlet: $T_1 = 500^\circ\text{C}$ and $p_1 = 240 \text{ bar}$ (i.e., super-critical conditions); if the discharge pressure is $p_2 = 40 \text{ bar}$, the isenthalpic temperature is $T_{2h} = 386.1^\circ\text{C}$, the isentropic temperature is $T_{2s} = 250.4^\circ\text{C}$ and the temperature found from Equation 5.1 is $T_2 = 318.2^\circ\text{C}$. This example becomes clearer in Figure 5.1 where we show the three transformations: the isenthalpic (green line), the isentropic (red line) and the one we obtain linking the thermodynamic points 1 and 2. It is important to note that the aforementioned hypotheses have

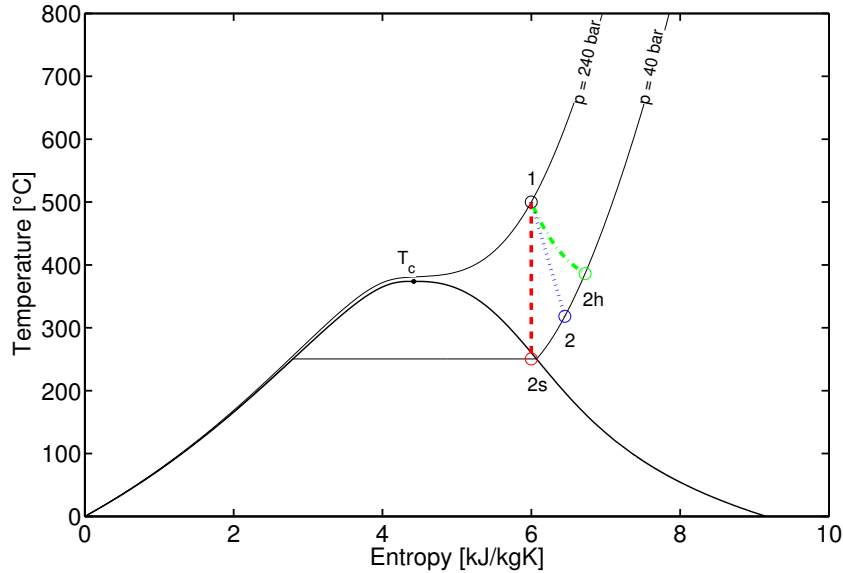


Figure 5.1 Thermodynamic process into the test section

a foundation; if the temperature of the steam that enters into the quenching chamber is not known *a priori*, the conditions of super-critical water at the test section inlet are accurately known (see Figure 3.1, “TTr-5”, visible on the calming chamber, consists of thermocouple with a low response time). Thus, knowing this information is sufficient to calculate T_{2s} and T_{2h} . Moreover, since $T_{2s} < T_2 < T_{2h}$, Equation 5.1 yields a good approximation of T_2 .

Finally, when available, experimental data has been used to validate the suggested hypothesis. What we observed from experimental data (Muftuoglu and Teyssedou, 2013) is that choked flow transformation is highly complex. Figure 5.2 shows the studied thermodynamic

conditions of the critical flow before the test section (blue points). In particular, we analyzed two conditions ($p_1 = 236.64 \text{ bar}$, $T_1 = 499.93^\circ\text{C}$ and $p_1 = 239.43 \text{ bar}$, $T_1 = 470.16^\circ\text{C}$) and, knowing the discharging pressure ($p_2 = 7.8 \text{ bar}$), we studied either the isoenthalpic (dash-dotted green lines) and the isoentropic (dashed red lines) transformations. Thereafter, we compared our calculation with the effective temperature at the test section outlet (star in the end of the dotted black line). As it can be seen, the transformation is neither isoenthalpic nor isoentropic, which means that the thermodynamic conditions of the steam cannot be described solely by one of these transformations. In effect, we conclude that with the information in our possession, it is not possible to formulate any hypothesis, other than the one proposed, to evaluate the steam temperature, since the choked flow transformation is not well defined.

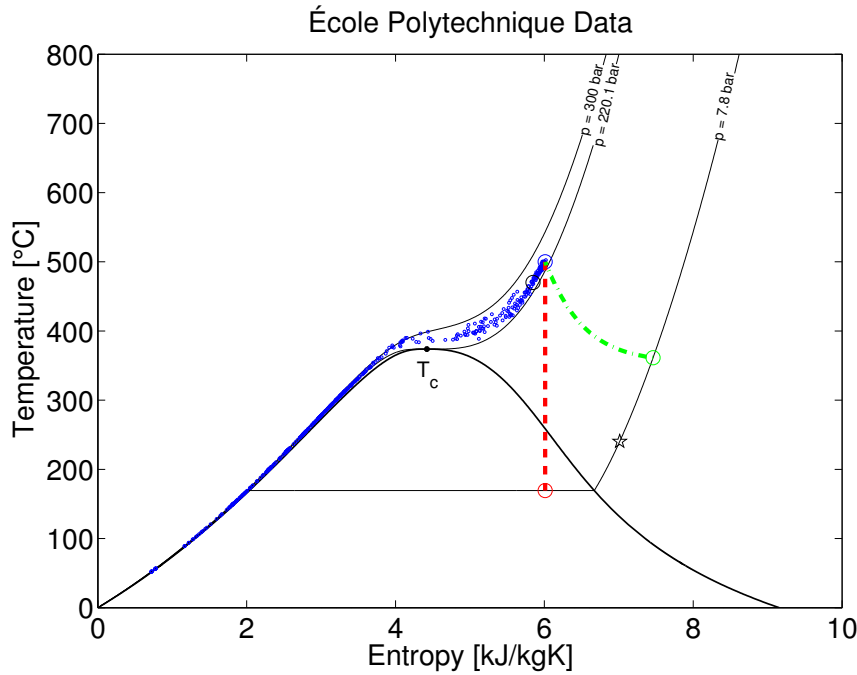


Figure 5.2 Choked flow experimental data (Muftuoglu and Teysseidou, 2013)

5.2 The Solution of the Heat Transfer Problem

Thus, for a given value of the liquid flow rate, the knowledge of the initial water temperature, the steam temperature given by Equation 5.1 and the droplet size distribution from Equation 4.14 should make it possible to determine the heat transfer between the steam and droplets. The overall procedure consists in analyzing droplets which varies in size between $D_{0.1}$ (Equation 4.17) and $D_{0.999}$ (Equation 4.18). Hence, for each droplet, we study the behav-

ior of the variables (which are functions of time) that affect the heat transfer. These variables are the droplet size (i.e., when evaporation occurs), the drag coefficient, the droplet velocity, the residence time, the heat transfer coefficient, the temperature and the evaporation rate. More details about the methodology are given in the following sections.

5.2.1 Droplet Convective Heat Transfer

The water entering into the quenching chamber (Figure 3.1) is at sub-cooled state while the steam may be at saturation or super-heated. Therefore, during the first interaction of droplets with the steam, heat is transferred to the liquid only by convection (Cascella and Teyssedou, 2013). Let us assume that the temperature distribution inside a spherical droplet of radius R can be determined from a conduction heat transfer equation written in spherical coordinates as (Ozisik, 1993):

$$\frac{\partial^2 T}{\partial r^2} + \frac{2}{r} \frac{\partial T}{\partial r} = \frac{1}{\alpha} \frac{\partial T}{\partial t} \quad (5.2)$$

where the temperature depends on the droplet radius r and on time t (i.e., the effects of others spatial coordinates are neglected). To solve this equation, the following boundary conditions are imposed:

- Uniform initial temperature distribution inside the droplet, $T(r, 0) = T_i$;
- Continuity of the heat flux at the droplet surface, $-k_l \frac{\partial T}{\partial r} \Big|_{r=R} = h[T(R, t) - T_\infty]$;
- Symmetry at the center of the droplet, $\frac{\partial T}{\partial r} \Big|_{r=0} = 0$.

Figure 5.3 shows the droplet control volume and the aforementioned boundary conditions.

The convective heat transfer coefficient h is estimated using the Ranz and Marshall correlation expressed as (Marshall, 1955):

$$Nu = \frac{hD}{k} = 2 + 0.6Re_v^{1/2} Pr^{1/3} \quad (5.3)$$

where Re_v is the steam Reynolds number based on an observer moving with respect to the steam at the velocity of the droplets.

Equation 5.3 requires a previous knowledge of the droplet velocity (i.e., value of Re_v) that is obtained by solving the following problem (Takahashi *et al.*, 2001):

$$\begin{cases} \rho_l \frac{\pi D^3}{6} \frac{dv_D}{dt} = 3\pi\mu_v D f \mathbf{v} + \rho_l \frac{\pi D^3}{6} g & t > 0 \\ v_D = \frac{\dot{V}_{liq}}{\pi d_0^2/4} & t = 0 \end{cases} \quad (5.4)$$

where v_D is the droplet velocity, \mathbf{v} is the relative velocity, f is a drag factor and g is the acceleration of gravity. Assuming that the steam velocity is close to zero, we considered that $v_D \cong \mathbf{v}$. As usual, the drag factor is calculated as a function of the drag coefficient C_D and

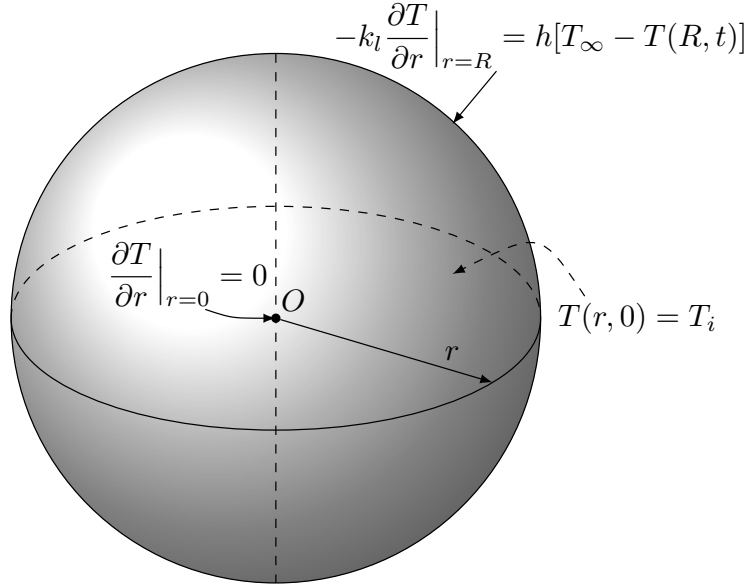


Figure 5.3 Droplet control volume

the Reynolds number Re_v , as:

$$f = \frac{C_D Re_v}{24} \quad (5.5)$$

Ashgriz (2011) provides an experimental correlation for spray droplets given by:

$$\begin{cases} C_D = \frac{24}{Re_v}(1 + 0.15Re_v^{0.687}) & Re_v \leq 10^3 \\ C_D = 0.44 & Re_v > 10^3 \end{cases} \quad (5.6)$$

Only close to the nozzle the Reynolds number Re_v is higher than 10^3 (Beck and Watkins, 2002). The iterative method used to study Equation 5.4 (i.e., Runge-Kutta) slowly converges to the solution. Thus, instead of solving Equation 5.4, we assume that the droplet quickly reaches the terminal velocity. That is, the droplet velocity can be estimated as:

$$v_D = \frac{g\tau_v}{f}, \quad \tau_v = \frac{\rho_l D^2}{18\mu_v} \quad (5.7)$$

where τ_v is defined as the velocity response time. In Figure 5.4 we validate this hypothesis by studying the velocity trend of a $100 \mu\text{m}$ freely falling droplet in a super heated steam environment (the droplet has constant temperature and evaporation has not been considered). The velocity trend is calculated solving Equation 5.4 and 5.7. As we can see, the error committed using the approximation is remarkable only at the initial time and it rapidly goes to zero.

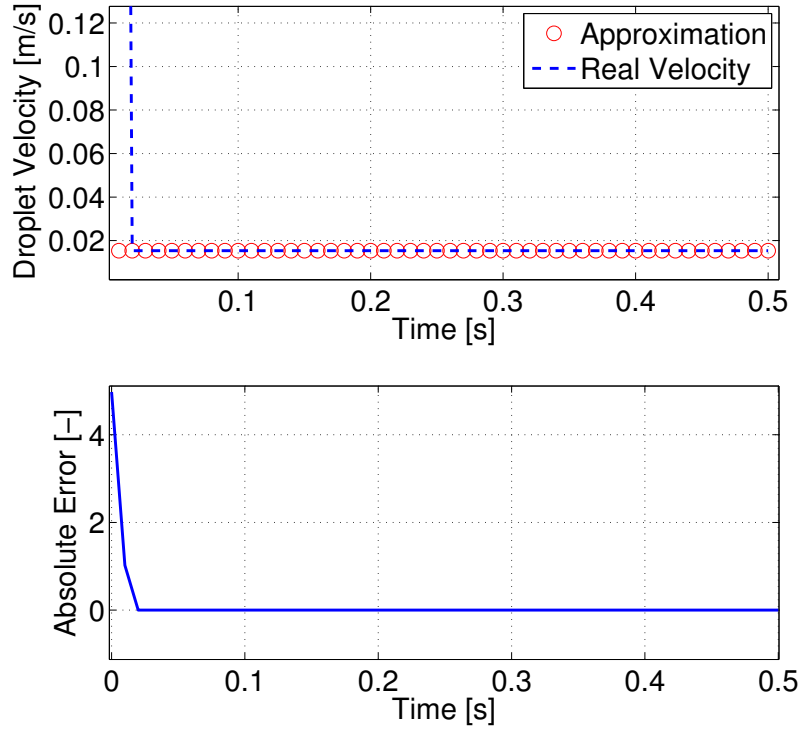


Figure 5.4 Comparison between the real velocity trend and the approximation

Knowing the boundary conditions, Equation 5.2 is now solved using the method of separation of variables (the details are given in Appendix B), which gives (Incropera *et al.*, 2007):

$$\frac{T(r, t) - T_\infty}{T_i - T_\infty} = \sum_{n=1}^{\infty} \frac{4[\sin \zeta_n - \zeta_n \cos \zeta_n]}{2\zeta_n - \sin 2\zeta_n} e^{-\zeta_n^2 Fo} \frac{\sin \zeta_n \mathbf{r}}{\zeta_n \mathbf{r}} \quad (5.8)$$

where \mathbf{r} is the dimensionless diameter defined as $\mathbf{r} = r/R$, Fo is the Fourier number and ζ_n are the roots of the following equation:

$$1 - \zeta_n \cot \zeta_n = Bi \quad (5.9)$$

and Bi the Biot number. However, we are not interested in the temperature profile but we want to know the mean temperature of the droplets. Schneider (1955) provides the space-averaged solution of the heat transfer problem with the mean temperature obtained from:

$$\bar{T} = \frac{1}{\frac{4}{3}\pi R^3} \int_0^R 4\pi r^2 T, dr \quad (5.10)$$

The complete solution of Equation 5.2 is expressed as (Schneider, 1955):

$$\frac{\bar{T} - T_\infty}{T_i - T_\infty} = \sum_{n=1}^{\infty} \frac{6}{\zeta_n^2} \frac{[\sin \zeta_n - \zeta_n \cos \zeta_n]^2}{\zeta_n - \sin \zeta_n \cos \zeta_n} e^{-\zeta_n^2 Fo} \quad (5.11)$$

In this work, we have used only the first five roots of Equation 5.9 (listed in Appendix C) taken from the Schneider (1955). The energy transferred by convection in time t^* can be estimated as:

$$Q_{conv}(t^*) = \frac{\pi D^3}{6} \int_{\bar{T}_i}^{\bar{T}(t^*)} \rho_l(\bar{T}) c_{p,l}(\bar{T}) d\bar{T} \quad (5.12)$$

It is obvious that under a particular set of experimental conditions, the heat transfer problem can be simplified. For instance, when $Fo > 0.2$, the solution of Equation 5.2 can be approximated by considering only the first term of Equation 5.11 which leads to:

$$\frac{\bar{T} - T_\infty}{T_i - T_\infty} = \frac{6}{\zeta_1^2} \frac{[\sin \zeta_1 - \zeta_1 \cos \zeta_1]^2}{\zeta_1 - \sin \zeta_1 \cos \zeta_1} e^{-\zeta_1^2 Fo}$$

with ζ_1 the first root of Equation 5.9. In turn, if $Bi \ll 0.1$, the lumped parameter approach can be applied and gives (Incropera *et al.*, 2007):

$$\frac{\bar{T} - T_\infty}{T_i - T_\infty} = e^{-\frac{t}{\tau_T}}$$

with

$$\tau_T = \frac{\rho_l V_D c_{p,l}}{h A_s} \quad (5.13)$$

5.2.2 Droplet Evaporation Heat Transfer

When droplets reach saturation conditions, they start evaporating (Cascella and Teyssedou, 2013). Marshall (1955) has studied the evaporation of sub-cooled droplets in a hot-air environment. Assuming that the heat transferred to a droplet from steam by convection vaporizes the droplet itself, then for a single droplet the following energy balance equation can be written:

$$h\pi D^2 [T_v - T_s] dt = dm_{evap} h_{fg}$$

with h_{fg} the latent heat of vaporization. This equation allows the rate of mass transferred to the steam to be calculated as:

$$\dot{m}_{evap} = \frac{dm_{evap}}{dt} = \frac{h\pi D^2 [T_v - T_s]}{h_{fg}} \quad (5.14)$$

It is apparent that this mass transfer plays an important role in the physics of the problem. In fact, the value of \dot{m}_{evap} provides a direct indication of the amount of thermal energy that is transferred along the phase change process taking place in the droplets. Equation 5.14 shows that \dot{m}_{evap} depends on the diameter of the droplet D which decreases while increasing the evaporation rate, and the heat transfer coefficient h , both of which are functions of time. Therefore, it cannot be assumed that the evaporation rate will be the same for each droplet at each time step. Hence, the droplet-mass variation can be expressed as a function of time t :

$$\Delta m(t) = \int_{t_i}^t \frac{h(\tau)\pi D(\tau)^2 [T_v - T_s]}{h_{fg}} d\tau \quad (5.15)$$

where τ is the temporal variable of integration. Knowing the mass variation, the calculation of the energy released by phase change in the interval $t_f - t_i$ is straightforward:

$$Q_{evap} = \int_{t_i}^{t_f} \dot{m}_{evap}(t) h_{fg} dt \quad (5.16)$$

5.3 Thermal Power Transferred in DCHX Systems

For a droplet having known dimensions and thermal conditions, the knowledge of the thermal energy transferred by a single droplet comes from Equations 5.12 and 5.16:

$$Q_i = Q_{conv} + Q_{evap} = \frac{\pi D_i^3}{6} \int_{\bar{T}_i}^{\bar{T}(t^*)} \rho_l(\bar{T}) c_{p,l}(\bar{T}) d\bar{T} + \int_{t^*}^{t_f} \dot{m}_{evap}(t, D_i) h_{fg} dt \quad (5.17)$$

However, we are not interested in the energy released but rather in the total power exchanged under a set of given conditions (i.e., the conditions are studied in Section 6.1). This parameter can be found as follows:

$$\dot{Q}_{TOT} = \sum_{i=1}^n \dot{N}_i Q_i \quad (5.18)$$

where \dot{Q}_{TOT} is the total thermal power exchanged in the *DCHX*, \dot{N}_i is the rate of droplet population having diameter D_i and Q_i is the thermal energy found using Equation 5.17. For a given droplet diameter, the droplet population is determined by:

$$N_i = f_i(D_i) N_{TOT} \quad (5.19)$$

where N_i is the number of droplets with diameter D_i , N_{TOT} is the total number of analyzed droplets (both at steady state conditions) and f_i is the probability density function expressed

as:

$$f_i(D_i) = \left. \frac{dF(D)}{dD} \right|_{D=D_i} \quad (5.20)$$

It is obvious that this probability density function corresponds to the derivative of the cumulative probability given by Equation 4.14 and can be evaluated by assuming steady state conditions as (Cascella and Teyssedou, 2013):

$$f_i(D_i) = \frac{N_i}{N_{TOT}} = \frac{\dot{N}_i \delta t}{\dot{N}_{TOT} \delta t} \quad (5.21)$$

The total flow rate of droplets can be estimated by the following expression:

$$\dot{N}_{TOT} = \frac{6\dot{V}_{liq}}{\pi D_m^3} \quad (5.22)$$

where D_m is the mean statistical diameter of the droplets. Then, from Equation 5.18, the total thermal power becomes:

$$\dot{Q}_{TOT} = \sum_{i=1}^n \dot{N}_i Q_i = \dot{N}_{TOT} \sum_{i=1}^n f_i(D_i) Q_i \quad (5.23)$$

where n is the number of droplets from Equation 6.1 (Cascella and Teyssedou, 2013).

5.4 Final Remarks on the Presented Procedure

In this chapter the heat transfer procedure has been presented. In developing it, we tried to follow as much as possible a clear and rigorous method to calculate the thermal power. In spite of that, this procedure can be questionable.

First of all, the evaluation of steam temperature is not precise; experience shows that our hypothesis (Equation 5.1) can be, in some situations, completely unsubstantiated (Figure 5.2). However, the phenomena concerning the choked flow make the task of evaluating this temperature quite difficult. Moreover, the latter is assumed constant during the direct contact with liquid droplets; of course, this cannot be true. This hypothesis has been used since it is highly difficult to characterize the heat transfer between two mixing fluids: therefore, we must point out that this assumption will lead to an overestimation of the experimental data.

Another questionable point is related to the study of droplet evaporation. In fact, when a droplet reaches saturation conditions, the surrounding steam may condensate on its surface. This problem has been studied in detail; nevertheless, the choice of choosing droplet evaporation instead of steam condensation is based on the following considerations:

- If evaporation occurs, the droplet needs energy in order to change its phase, since it is an endothermic process and this energy can come only from steam. Thus, the rate of evaporation corresponds to Equation 5.14;
- If condensation occurs, this means that the steam is transferring energy to the droplets. Since it is an exothermic process, also the rate of steam condensation can be approximated as:

$$\dot{m}_{cond} = \frac{dm_{cond}}{dt} = \frac{h\pi D^2 [T_v - T_s]}{h_{fg}} \quad (5.24)$$

it is obvious that the use of this equation will increase the droplet sizes, instead of decreasing them.

We did our calculations assuming that these two scenarios were valid and we discovered that the final evaluated thermal power does not change at all. For this reason, we chose the scenario that corresponds to evaporation, which according to us was more plausible. However, this topic still remains open to discussions.

Finally, the assumption of matching the probability density function to the droplet flow rate ratio (Equation 5.21) is valid only under steady state conditions, where the DDF does not change in time. Since the conditions of steam coming from the test section were not stable, the liquid flow rate is never constant and, from a theoretical standpoint, Equation 5.21 should not be used.

In the next chapter, we will analyze the data collected under the experimental facility . Further, the predictions of our model are compared the data.

CHAPTER 6

RESULTS

The experimental data collected in our laboratory has been used to validate the modeling approach presented in Chapter 4 and 5. For this reason, we present here a comparison between the experimental data and the predictions of the model. However, we do not limit ourselves to this task.

The chapter begins by explaining how the model works and also presents its flow diagram (Section 6.1). Afterwards, we focus our attention on how it implements the properties necessary to evaluate the total thermal power for a prescribed set of thermodynamic conditions. Also, we will highlight how the droplet dimensions may affect the quenching chamber behavior. In turn, the predictions are compared with the experimental data collected for three different quenching chamber pressures (Section 6.2). Since there are discrepancies between predictions and data, it is essential to understand where these differences come from. In effect, a parametric study which focuses on how two parameters, the quenching chamber pressure and the liquid flow rate, influence the prediction of the model is performed (Section 6.3). From this, we will draw our conclusions by providing a corrective coefficient that improves the model.

6.1 Model Methodology

The methodology presented in Chapter 4 and 5 has been used to develop a computer model for which the flow diagram is presented in Figure 6.1. As it can be seen, to perform our simulations, it is necessary to provide the variables that describe the DCHX working conditions, i.e., the steam temperature at the test section inlet T_v , the quenching chamber pressure P_{qch} , the cooling liquid temperature $T_{liq,i,j}$ ¹ and its volumetric flow rate \dot{V}_{liq} . Knowing this information, it is possible to evaluate the Sauter mean diameter D_{32} from Equation 4.5 and, for a given value of q , the DDF from Equation 4.14. Thus, Equations 4.17 and 4.18 have been used in order to generate n droplets having diameters ranging from $D_{0.1}$ to $D_{0.999}$:

$$n = \frac{D_{0.999} - D_{0.1}}{dD} \quad (6.1)$$

1. Here, the index i stands for the time variable, while j for the droplet dimension; this aspect will become clearer, when the matrix $\mathbf{P}_{m,n}$ will be presented

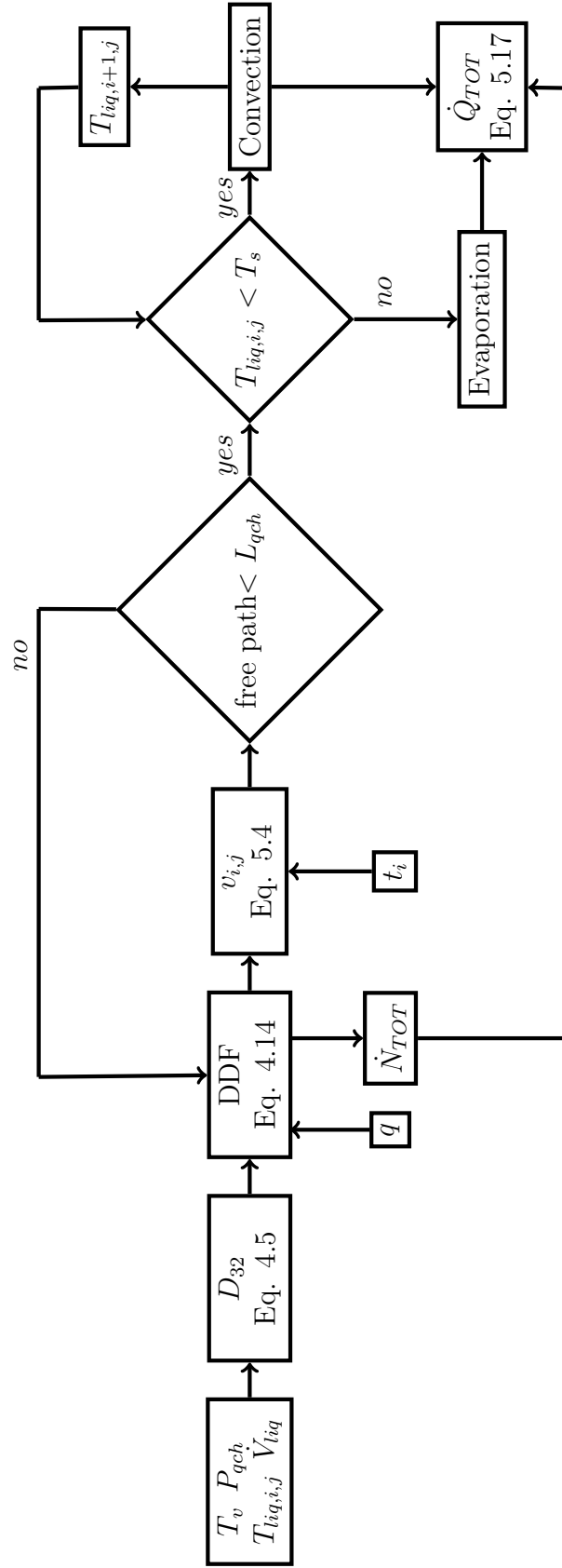


Figure 6.1 Model flow diagram

with $dD = 10^{-6}m$. Consequently, the probability of having a diameter D_j (with $D_{0.1} < D_j < D_{0.999}$) is evaluated differentiating the cumulative distribution function. Thereafter, a temporal scale with a time step of 10 *ms* is applied in such a way that for each diameter and time increment the droplet velocity $v_{i,j}$ is calculated (Equation 5.4). In effect, this is necessary not only to predict convection heat transfer but also to calculate the droplet residence time in the chamber. In fact, since the size affects their velocity, the biggest droplets will reach the bottom of the quenching chamber faster than smaller and mean ones. For instance, if a droplet of diameter D_j has a velocity $v_{i,j}$ and a residence time in the chamber t_i , the droplet free path is $s_{i,j} = v_{i,j}t_i$, and if this quantity is higher than the quenching chamber length (L_{qch} in Figure 6.1), the model will stop to analyze the droplet of size D_j to study the droplet of size D_{j+1} . After this analysis, the heat transfer study is performed starting by the evaluation of the droplet temperature. In fact, until it reaches saturation, convection heat transfer is considered, according to the methodology presented in Section 5.2.1. However, if the droplet temperature is equal to the saturation temperature T_s , evaporation heat transfer is studied (Section 5.2.2). Finally, the knowledge of the statistical distribution, the total rate of droplets \dot{N}_{TOT} and the heat exchanged by convection/evaporation makes it possible to determine the total power exchanged in the DCHX.

In order to perform the heat transfer study, the behavior of the properties presented in Sections 5.2.1 and 5.2.2 must be known; these are the drag factor, the heat transfer coefficient, the non-dimensional numbers (Nu , Re , Pr) and the evaporation rate. For this reason, the calculations has been developed in such a way that, as the simulation is running, the trend of each property is stored in a $m \times n$ matrix, namely $\mathbf{P}_{m,n}$, where m is the length of the temporal scale and n is the number of droplets:

$$\mathbf{P}_{m,n} = \begin{pmatrix} P(D_1, t_1) & P(D_2, t_1) & \cdots & P(D_n, t_1) \\ P(D_1, t_2) & P(D_2, t_2) & \cdots & P(D_n, t_2) \\ \vdots & \vdots & \ddots & \vdots \\ P(D_1, t_m) & P(D_2, t_m) & \cdots & P(D_n, t_m) \end{pmatrix} \quad (6.2)$$

It is important to mention that not all the elements of the matrix $\mathbf{P}_{m,n}$ contains a physical value. In fact, the residence time of a droplet D_j , as $1 < j < n$, is t_k , with $1 < k < m$. Also, this time is always lower than t_m and it is not equal for all droplets since the residence time depends on the thermodynamic conditions and size. For instance, because of its limited mass, a small droplet quickly vaporizes and so its residence time is shorter. However, a big droplet subjected to a low drag force (Equation 5.6) travels at high velocity, which means that it has a little residence time also. Finally, mean size droplets have a size which allows them to slowly vaporize and travel at mean velocity. However, if the residence time of a droplet D_j is

t_k , the element $P(i, j)$ of the matrix $\mathbf{P}_{m,n}$ is a finite value for $i < k$. Consequently, it is not defined for $i > k$ (i.e., it is zero).

In order to understand not only the aforementioned aspects but also the behavior of different droplets (roughly mentioned previously), a thermodynamic DCHX condition will be analyzed and the predictions will be presented in the next section.

6.1.1 Analysis of a DCHX Thermal Condition

Here we analyze the DCHX working condition summarized in Table 6.1. In particular, we highlight the choice of a mean value for q ($q = 2.4$) in Equation 4.14. For these conditions, we will analyze the velocity, the temperature and finally the energy released as a function of the droplet dimension and residence time.

Table 6.1 Parameters used to generate Figures 6.2, 6.3 and 6.5

Quenching Chamber Working Conditions	
Chamber pressure	$P_{qch} = 30bar$
Liquid flow rate	$\dot{V}_{liq} = 2 \times 10^{-5}m^3/s$
q value of Equation 4.14	$q = 2.4$
Steam temperature at test section inlet	$T_v = 340^\circ C$

Figure 6.2 shows the droplet velocity as a function of time and droplet size. As we can see, small droplets have an initial low velocity, while increasing the size their initial velocity increases; in fact, the drag force acting on droplets diminishes with increasing the size. Moreover, it is clear from Figure 6.2 that the residence time of small droplets is low (in fact, until the droplet does not vaporize the model keeps on evaluating the velocity). As their size increases, the droplet residence time also increases (in fact, the model evaluates the velocity of mean size droplets at times greater than $0.5s$). Finally, when the droplet dimension reaches a critical value (i.e., $320 \mu m$), its residence time decreases with the size. This behavior can be explained in the following way. Small size droplets have a low mass, this means that they rapidly vaporize. Thus, the fact that these droplets travel at a low velocity (which comes from the high drag coefficient from Equation 5.6) is not a sufficient condition to augment the residence time. Increasing the size brings up the mass and leads to a higher time needed to vaporize. However, if the droplet has a diameter higher than the critical value (i.e., $D_{cr} = 320\mu m$), it will have a low residence time because their velocity is too high (Figure 6.2). In fact, for bigger droplets, the influence of the velocity is too strong and the drop in size due to evaporation is not enough to increase the residence time. This means that big droplets travel at a high enough velocity to rapidly reach the bottom of the

quenching chamber without completely vaporizing. Thus, the trade-off between droplet size and velocity which maximizes the residence time with $D_{cr} = 320\mu m$ is obvious.

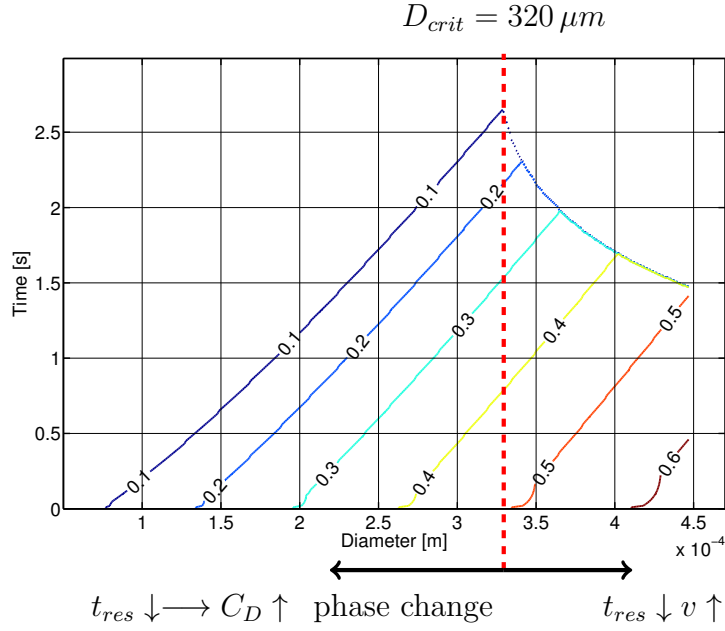


Figure 6.2 Parametric velocity (in m/s) as a function of time and droplet size

This apparent trade-off is shown as a function of the droplet temperature, size and time in Figure 6.3. In this case, the temperature is evaluated as a function of the residence time. Because small size droplets vaporize faster, the temperature change within short periods of times. The droplet residence time increases with droplet size. It reaches critical value and then start decreasing. For instance, for a droplet of diameter D_j at time t_i , if the model is not able to provide the residence time for the temperature $T_{liq,i,j}$, this means that one of the following situations occur:

- The droplet mass is completely vaporized ($D_j < D_{cr}$),
- The droplet has reached the bottom of the quenching chamber ($D_j > D_{cr}$).

Several aspects can be highlighted from Figure 6.3. First of all, every single droplet reaches the constant temperature of saturation (the plateau clearly shown in figure). Secondly, it is possible to distinguish both aforementioned heat transfer modes, namely convection and evaporation. In fact, if the droplet of diameter D_j is subjected to an increase in temperature during the time interval $t_{i+1} - t_i$, this means that convection is taking place. On the other hand, if the temperature stops changing, the heat transfer mechanism is driven by evaporation. In particular, it is clearly shown the effect of droplet size on convection: small droplets rapidly reach saturation temperature while the bigger ones undergo a smoother change in

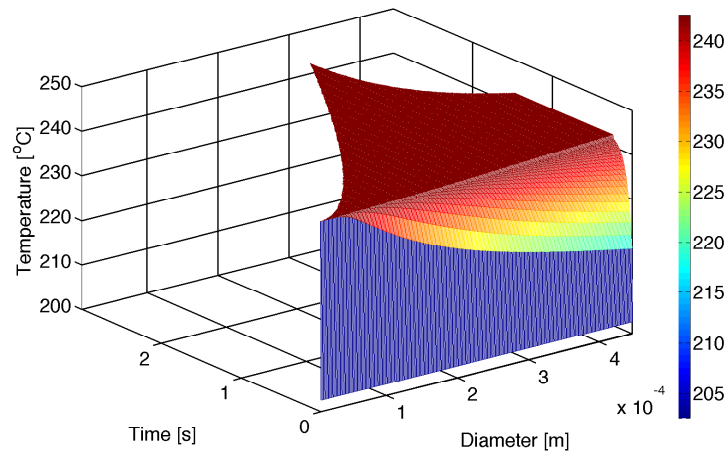


Figure 6.3 Temperature field

temperature. This aspect could be predicted even before simulations are performed. Let us define the energy capacity of a droplet C as the product of its mass m_D and the heat capacity at constant pressure c_p

$$C = m_D c_p$$

At first glance, for a given set of thermodynamic liquid conditions, the droplet energy capacity depends only on the mass i.e., the higher the mass, the higher the capacity of a

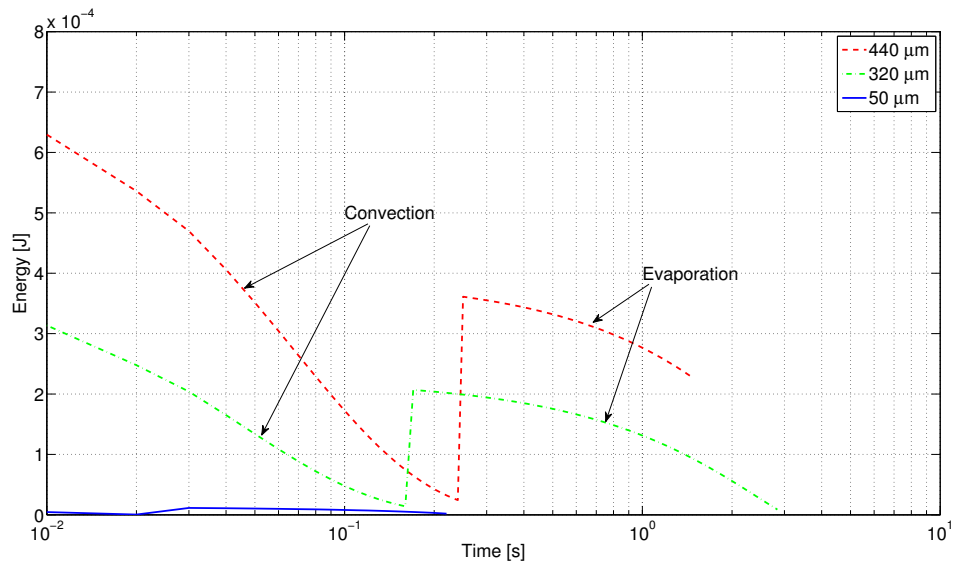


Figure 6.4 Energy released from droplets as a function of residence time

droplet of exchanging energy becomes. For this reason, bigger size droplets need more time to reach saturation, when compared with smaller size droplets. This is the reason why the temperature change is smoother for large droplets (even if the initial temperature is the same for all droplets).

Since droplets exchange energy both by convection and evaporation, it is useful to show the respective weight of these two contributions. In Figure 6.4 we plot the energy absorbed by three different size droplets as a function of the residence time (on a logarithmic-time scale). For a small size droplet, the energy is negligible but becomes more significant as the dimension increases. Moreover, it is possible to discern convection and evaporation heat transfer modes for big and mean size droplets. At the beginning, when the temperature difference between the liquid and the gas is considerable, the energy absorbed by convection is also important but decreases when the droplet temperature approaches saturation. Once the saturation is reached, evaporation occurs and leads to a larger heat transfer due to the mass transfer. From Figure 6.4, we must point out that not only the difference in residence time due to droplet dimension but even the time at which evaporation occurs increases with increasing the size. In fact, as mentioned in the previous paragraph, big size droplets reach saturation later than small size ones, due to higher convection contributions from big size droplets.

Finally, Figure 6.5 shows the absorbed energy Q_{TOT} (Equation 5.17) as a function of the droplet size. Here we can see how this parameter increases with increasing the droplet dimension (as already shown in Figure 6.4). However, this growth is not constant. At the beginning, it seems that $Q_{TOT} \propto D^2$, which is equivalent to say that $Q_{TOT} \propto S_D$ where S_D is the droplet surface area. This means that the energy increases with increasing the contact surface area (which is obvious). But, after a certain point, this growth become linear, i.e., $Q_{TOT} \propto D$ which means that there is a phenomena taking place that makes the energy transfer to decrease. Comparing Figure 6.5 with Figure 6.2 and 6.3, it is possible to conclude that this change of behavior happens exactly at the critical size value of $D_{cr} = 320\mu\text{m}$, where the a high droplet velocity enable vaporization to occur. As already mentioned, droplets with a diameter larger than the critical value reach the bottom of the chamber before their complete vaporization. In fact, for high velocity, droplets have not enough time to transfer all their energy, leading to a decrease in the amount of energy. Based on this figure, we can draw our first conclusion about the DCHX efficiency; even if big droplets have higher energy capacity (C) than small droplets, they do not necessarily improve the overall quenching chamber efficiency. The highest efficiency has to be found in the optimum droplet velocity or, in other words, in the optimum volumetric flow rate that does not make any of the droplets reach the bottom of the quenching chamber before their complete vaporization occurs. That

is, there exist a value for the liquid flow rate that maximizes the amount of absorbed energy.

In this section, we highlighted the behavior of droplets in the quenching chamber, and we begun to understand how their size can affect the heat transfer process. This information is necessary to analyze the comparison between predictions and experimental data to be presented in the next section.

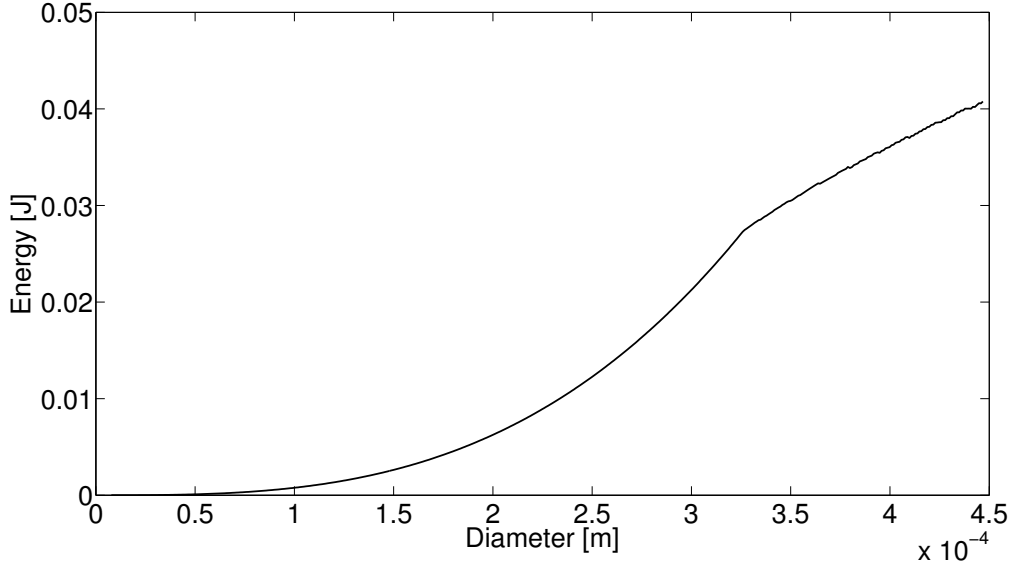


Figure 6.5 Energy released from droplets as a function of size

6.2 Comparison of Model with Experimental Data

In this section the predictions of the proposed modeling approach are compared with experimental data obtained using the facility shown in Figure 3.1. Data were collected for three values of steam pressure ($P_{qch} = 1.6 \text{ MPa}$, $P_{qch} = 2.1 \text{ MPa}$ and $P_{qch} = 3.1 \text{ MPa}$) over a wide range of water flow. Figure 6.6 shows a comparison of model predictions with data. These value do not take into account the negligible thermal losses to the environment.²

2. These losses can be evaluated knowing the thermal resistance:

$$R = \underbrace{\frac{1}{2h_i\pi r_1 L_{qch}}}_{\text{Liquid Film}} + \underbrace{\frac{\log(r_2/r_1)}{2\pi k_w L_{qch}}}_{\text{Conduction-Wall}} + \underbrace{\frac{\log(r_3/r_2)}{2\pi k_{is} L_{qch}}}_{\text{Conduction-Insulation}} + \underbrace{\frac{1}{2h_e\pi r_3 L_{qch}}}_{\text{Natural convection}}$$

The calculus of the thermal resistance requires an analysis on the heat transfer mechanism occurring on the internal wall (probably evaporation, since droplets may impact the wall of the chamber, forming a liquid layer) and on the external side of the DCHX wall (obviously natural convection). Assuming that the thermal losses are mainly due to the heat conduction across the thermal insulation of the quenching chamber leads to an overestimation of the thermal losses; moreover, our calculations have showed that the losses increase

The results presented in Figure 6.6 show that for low steam pressure ($P_{qch} = 1.6 \text{ MPa}$, $P_{qch} = 2.1 \text{ MPa}$), the agreement of the model with the data is very good. In spite of that, this is not necessarily true at high pressure ($P_{qch} = 3.1 \text{ MPa}$) where the proposed model significantly overestimates the thermal power.

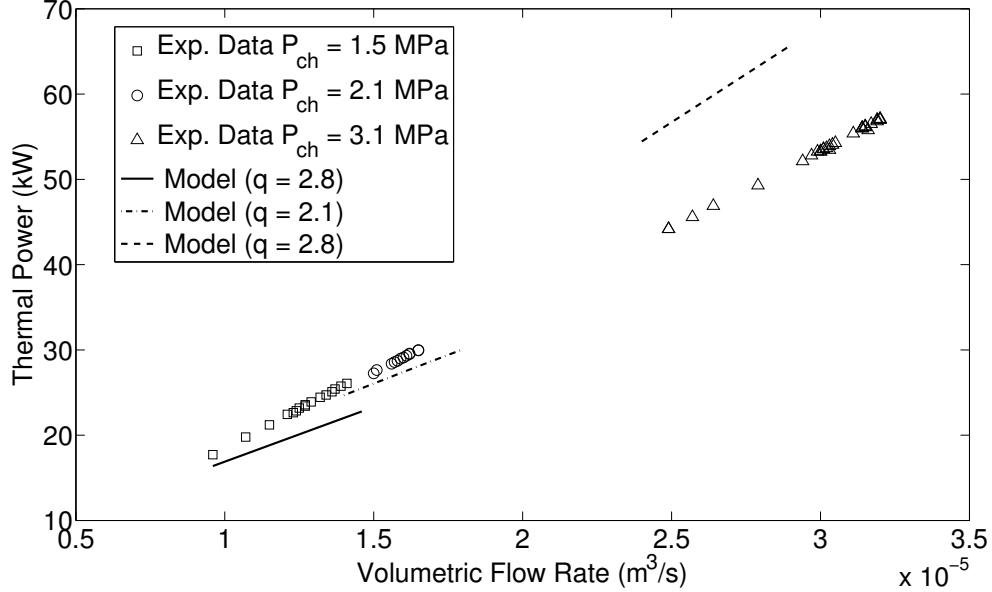


Figure 6.6 Comparison of model predictions with data

Several phenomena which are not taken into account in the present model can probably explain this behavior. One of these aspects has been mentioned in the previous section, where we highlighted how some droplets reach the bottom of the quenching chamber before their complete vaporization occurs, leading to a drop in the DCHX performance. However, droplets may impact even the inner wall of the quenching chamber. This kind of interaction may contribute to the formation of a liquid film on the inner side of the DCHX. This layer should move downward and, assuming steady conditions, it is continuously supplied by liquid droplets. Moreover, if the assumptions made in Section 5.4 are correct, the formed layer should evaporate. In this situation, the contact surface area is greatly reduced because a non negligible portion of the droplets feeds this inner water layer. On the other hand, the surface available to exchange heat is lower compared to a situation in which none of the droplets

with the DCHX working pressure. So, we evaluated them for $P_{qch} = 40 \text{ bar}$:

$$\dot{Q}_{Diss} = \frac{T_v - T_{amb}}{\frac{\log(r_3/r_2)}{2\pi k_{is} L_{qch}}}$$

which gives 240 W transferred to the environment. That is, the thermal losses are always lower than this value, and neglecting them does not provide any considerable error in our calculation.

are deposited over the wall (in fact, for a given liquid mass, the contact area is higher if this mass is under the form of tiny droplets instead of being an unique liquid sheet). It is obvious that a decrease in the total contact surface area leads to a decrease in heat transfer since the latter is proportional to the surface area³. The fact that our model overestimates the data at high pressures (Figure 6.6 and 6.9) can be explained because it does not take into account this possible droplet deposit over the wall. In fact, it has a greater probability of occurring at high pressures than at lower ones. This aspect is confirmed by the fact that increasing the pressure, also increases the liquid flow rate and yields an augmentation of the total rate of droplets \dot{N}_{TOT} (Equation 5.22). In other words, this means that the probability that a droplet reaches the cylindrical wall is higher at high pressure, and leads to a non-negligible loss in heat transfer that has not been included in the model.

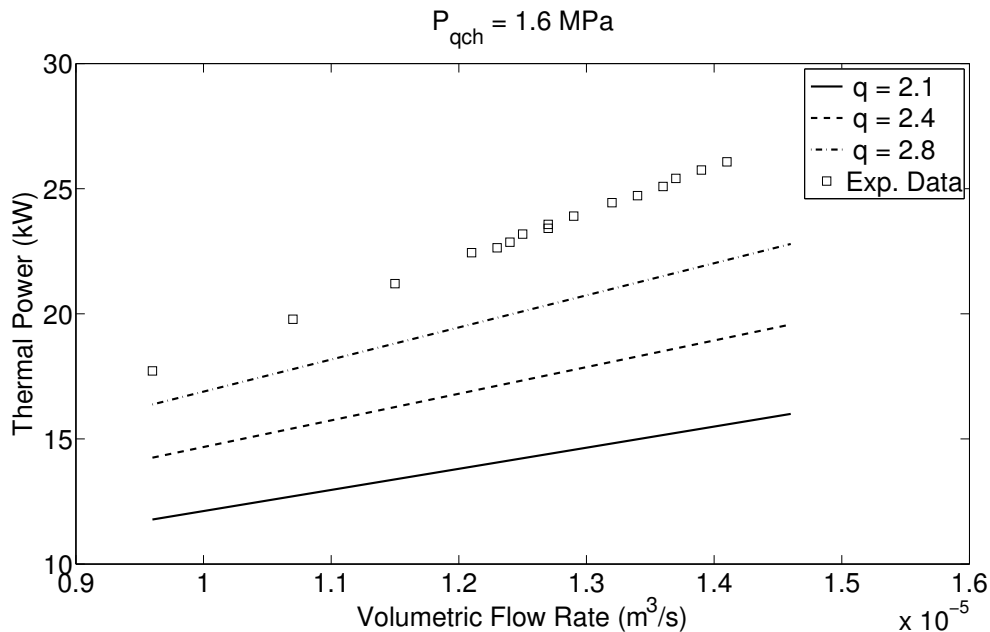


Figure 6.7 Model predictions ($P_{qch} = 1.6 \text{ MPa}$)

Another possible factor concerns the skewness of the DDF shown in Figure 4.4. In order to achieve a good agreement, the skewness has been optimized in Figure 6.6. However, this is not sufficient to reduce the gap at high pressures. Thus, a further analysis is needed to properly model this phenomena. Figure 4.4 indicates that for a constant skewness coefficient q , the pressure strongly affects the overall shape of the DDF. For instance, for a constant value of the Sauter mean diameter D_{32} (Equation 4.5), $D_{0.632}$ decreases with increasing q

3. This result should not be confused with what is shown in Figure 6.5. This figure states that the bigger the droplet size, the bigger the energy released becomes. Here we point out that increasing the total surface contact area (so, the sum of the areas of all the droplets), the heat transfer increases too.

(Equation 4.15). Consequently, the probability of obtaining droplets with small diameters increases (Equation 4.14). Recalling Figure 6.5, small size droplets exchange a negligible quantity of heat in contrast to big size droplets. However, for a fixed flow rate, the total number of droplets changes depending on the size of them. Indeed, the total number of droplet N_{TOT} is higher if their sizes are low (i.e., high value of q) and *vice versa* (i.e., low value of q). From Equation 5.23, we can argue that when q is increased (situation in which there is a large number of small size droplets), the heat transfer does not necessarily increases.

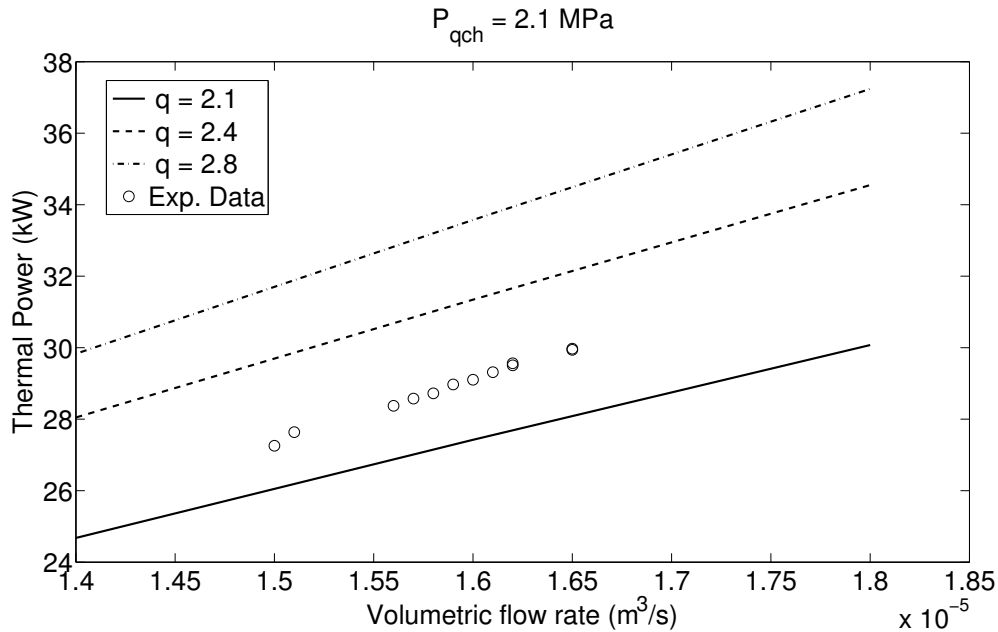


Figure 6.8 Model predictions ($P_{qch} = 2.1 \text{ MPa}$)

To better understand this aspect, the calculations shown Figure 6.6 were repeated using three values of q ($q = 2.1$, $q = 2.4$ and $q = 2.8$). These results are shown in Figures 6.7, 6.8 and 6.9. As it can be seen from these figures, at low pressures ($P_{qch} = 1.6 \text{ MPa}$, $P_{qch} = 2.1 \text{ MPa}$, where the agreement is good), increasing q increases the heat transfer. However, the same behavior is not observed at high pressure (Figure 6.9). To understand this change of behavior, we analyze the thermal power as a function of the quenching chamber pressure for the three different values of q (with the flow rate and the thermodynamic conditions of the water are fixed). In Figure 6.10, it is clearly shown that the thermal power does not increase linearly but, depending on q , there is a pressure that maximizes the heat transfer. Moreover, it seems that increasing q makes the maximal thermal power to shift to the right which explains the aforementioned trade-off between the droplet size (which decreases with pressure) and the total rate of droplets generation (which increases).

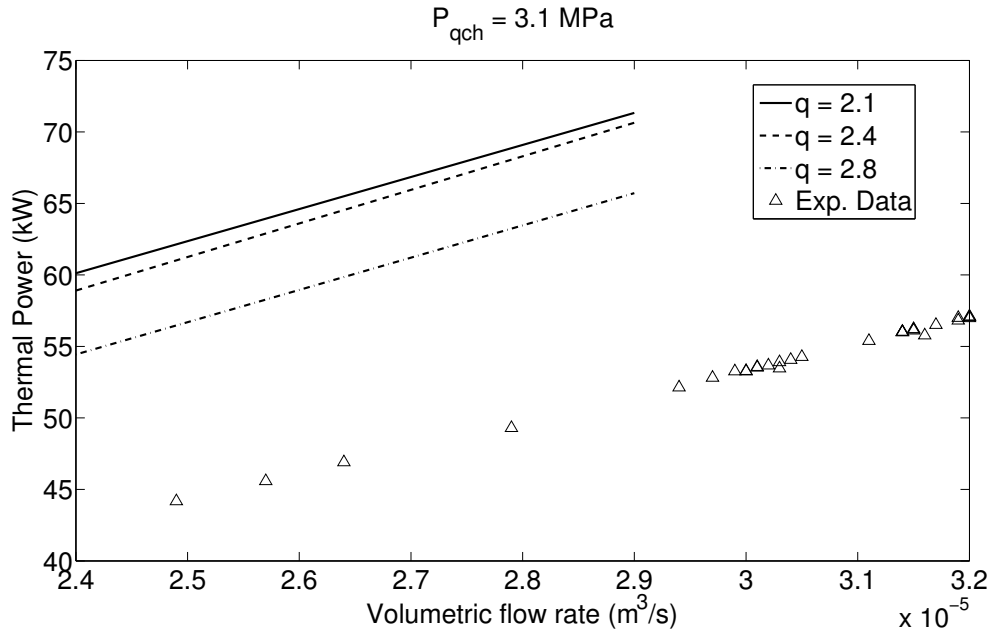


Figure 6.9 Model predictions ($P_{qch} = 3.1 \text{ MPa}$)

The fact that the thermal power is not a linear function of the pressure confirms analyses performed from Figure 6.5, where it is assumed the existence of a condition that maximizes the DCHX performance. In fact, it has been argued that for a given pressure, there is a value of the volumetric flow rate that optimizes the energy transferred from the droplets (it is the value that makes all the droplets completely vaporize before they reach the bottom of the chamber). Calculations shown in Figure 6.10 provide further information; for a given flow rate, the heat transfer does not linearly increase with pressure and, if the value of q is known, there is a DDF capable to maximize the heat transfer. Hence, to reach high heat transfer efficiencies, increasing the cooling flow rate may not be sufficient, therefore, it is necessary to find working conditions (i.e., a combination of flow rate and pressure) which provides the DDF that optimizes the quenching chamber performances. For this reason, in the next section we will neglect the influence of q to focus more on the effects of the volumetric flow rate and the quenching chamber pressure. However, as it has been shown, the effects of statistics (i.e., q) have a strong influence on heat transfer predictions, and this fact should never be forgotten.

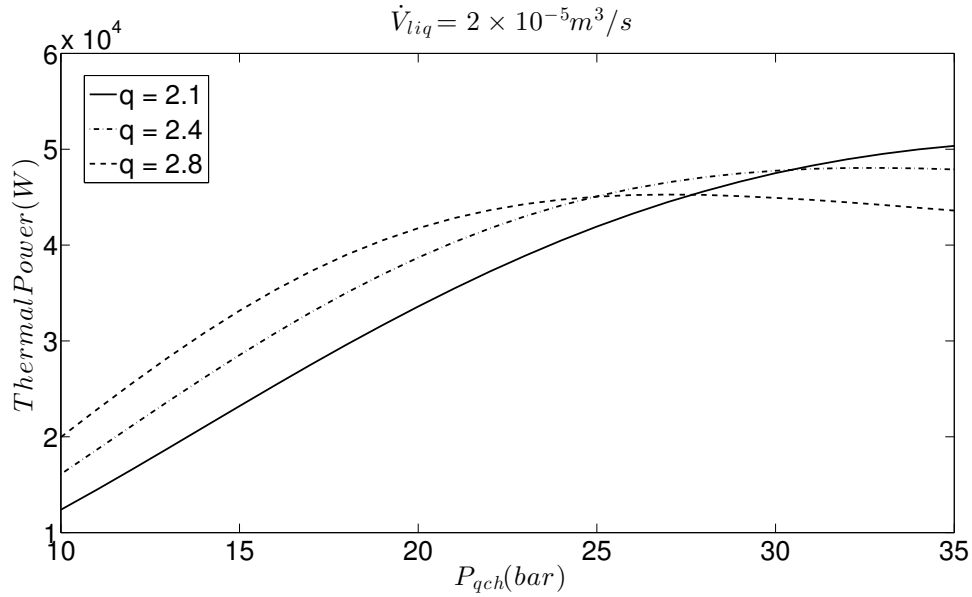


Figure 6.10 Heat transfer rate as a function of DCHX pressure P_{qch} and q

6.3 Parametric Study

If, on one hand, the behavior shown in Figure 6.10 highlights the effects of the droplet size distribution on heat transfer, on the other hand it represents an unrealistic situation. In fact, as said before, this figure has been evaluated keeping the volumetric flow rate constant and equal to a mean value. As shown in Figure 6.6, this situation never occurs and increasing the pressure requires an increment in the liquid flow rate in order to reach a good operation of the DCHX. The analysis made in the previous sections has shown that there are at least two

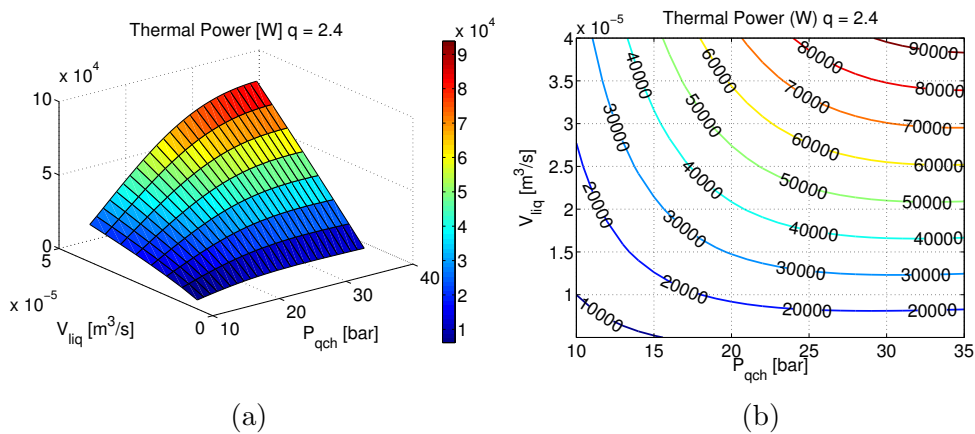


Figure 6.11 Heat transfer as a function of quenching chamber pressure P_{qch} and volumetric flow rate \dot{V}_{liq}

parameters that are more important than others that affect the behavior of the quenching chamber. For this reason, we focus our attention on the influence that the pressure and flow rate have on heat transfer predictions. Even though the statistics of the liquid droplets have a key role, calculations have been carried out by keeping q constant.

Figure 6.11 shows the DCHX thermal power as a function of the flow rate and the pressure for a constant value of q . Figure 6.11a shows that power increases with increasing these two variables. However, if we plot the contour curves of the thermal power as shown in Figure 6.11b, we deduce that the increase in power is not constant. In fact, it seems that under certain conditions, one of the two parameters has a greater effect on the calculations. For instance, when increasing the pressure, the influence on the heat transfer decreases. This is just one of the aspects that can be argued. However, in order to make a critical analysis of the results in Figure 6.11, a different representation is still needed.

Figure 6.12 presents the behavior of the thermal power for different values of the flow rate, as a function of the pressure. Obviously, increasing the cooling flow rate leads to a larger exchange in the thermal power. However, it is interesting to point out that, for low volumetric flow rates, the heat transfer is almost independent of the pressure while, increasing the liquid flow rate, the quenching chamber behavior changes, and is subjected to a remarkable dependence on pressure. Moreover, for each value of volumetric flow rate, the heat transfer does not grow linearly. That is, for a given flow rate, the thermal power increases with pressure; however, this growth is considerable at low pressures and not at high ones. Based on Figure 6.10, it can be argued that a maximum value for the heat transfer can be reached at high pressure.

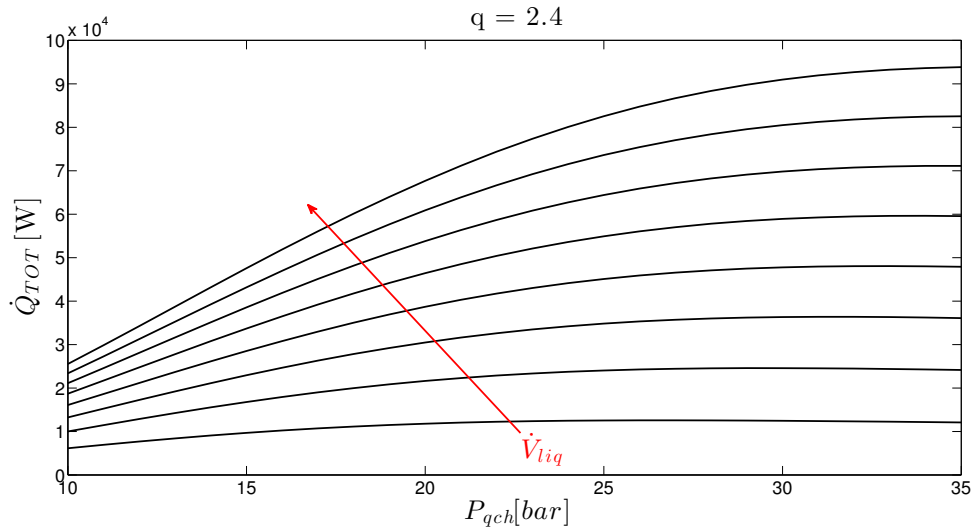


Figure 6.12 Influence of volumetric flow rate \dot{V}_{liq} on predictions

The same aspects can be seen in Figure 6.13, which shows the behavior of the thermal power for different values of working pressures. Again, the working pressure affects the quenching chamber behavior and, as aforementioned, the thermal power increases with increasing the pressure. However, it seems that, for a fixed flow rate, when certain values of pressure are reached (in this case, the highest ones), the thermal power does not increase anymore. That is, for a given volumetric flow rate, there exists a maximum thermal power that can be exchanged in the DCHX.

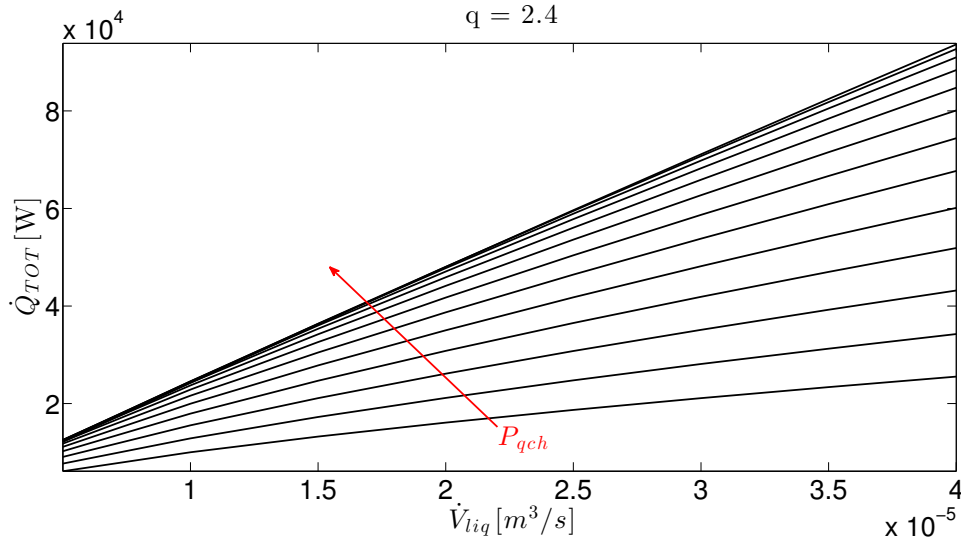


Figure 6.13 Influence of quenching chamber pressure P_{qch} on predictions

Figure 6.12 and 6.13 give us the directives to reach high heat transfer efficiencies. These two figures show that, in any case, an increment in the cooling water flow rate leads to an increment in heat transfer. But this increment depends on the chamber pressure as well, since an increment in heat transfer due to the flow rate seems to be higher if the pressure is high as well (Figure 6.12). This observation does not necessarily mean that an increment in pressure always results in a significant increase of the amount of heat transferred. In fact, this contribution becomes lower with increasing the pressure (Figure 6.13). The reasons of this behavior should be found in the effects that these two variables have on the droplet size. That is, increasing the pressure and decreasing the cooling water flow rate leads to a decrease in droplet size (Figure 4.2). It is obvious that the droplet size affects the heat transfer calculations; however, the model predictions have shown that under certain conditions, the heat transfer seems to be constant. This behavior can be justified by assuming that at these conditions, the cooling water flow rate and the quenching chamber pressure does not affect the droplet size at all. Consequently, the heat transfer predictions will be slightly influenced by these variables.

6.4 Other Correlation Approach

To improve our model, we decided to analyze Figure 6.13 in order to evaluate a generic function able to describe the predictions for $q = 2.4$. That is, this generic function f should have the quenching chamber pressure P_{qch} and the volumetric flow rate \dot{V}_{liq} as independent variables, and the thermal power \dot{Q}_{TOT} as a dependent variable. Then, using the experimental data, we will try to define a correction factor ψ which is a function of the pressure in order to achieve a better agreement. Let us define

$$\psi = \psi(\mathbf{p}), \quad \mathbf{p} = \frac{p}{p_{max}} \quad (6.3)$$

where \mathbf{p} is the non-dimensional pressure which is defined as the ratio between the quenching chamber pressure and the maximum allowable pressure, worth 40 *bar* in this case. Once this correction factor has been defined, the thermal power will be evaluated as

$$\dot{Q}_{TOT} = \psi(\mathbf{p}) f(P_{qch}, \dot{V}_{liq}) \quad (6.4)$$

The determination of f and c is presented in the two following subsections.

6.4.1 Definition of f

Let us assume that the curves in Figure 6.13 can be characterized by the following second-degree polynomial:

$$\dot{Q}_{TOT} = f(P_{qch}, \dot{V}_{liq}) = a\dot{V}_{liq}^2 + b\dot{V}_{liq} + c$$

where the coefficients a , b and c depend on pressure as follows

$$a = a(p) \quad b = b(p) \quad c = c(p)$$

The trend of a , b and c can be found by evaluating the coefficients of the second-degree polynomial describing the lines in Figure 6.13 and finally analyzing their dependence in pressure. Assuming that third-degree polynomials can describe the trend of a , b and c , we computed the following expressions:

$$a(p) = -8.8454 \times 10^8 p^3 + 9.371 \times 10^{10} p^2 - 2.6305 \times 10^{12} p + 1.2883 \times 10^{13}$$

$$b(p) = -2.5258 \times 10^4 p^3 - 2.2061 \times 10^6 p^2 + 2.0845 \times 10^8 p - 1.0860 \times 10^9$$

$$c(p) = 0.7813 p^3 - 55.5 p^2 + 1.0853 \times 10^3 p - 3.5098 \times 10^3$$

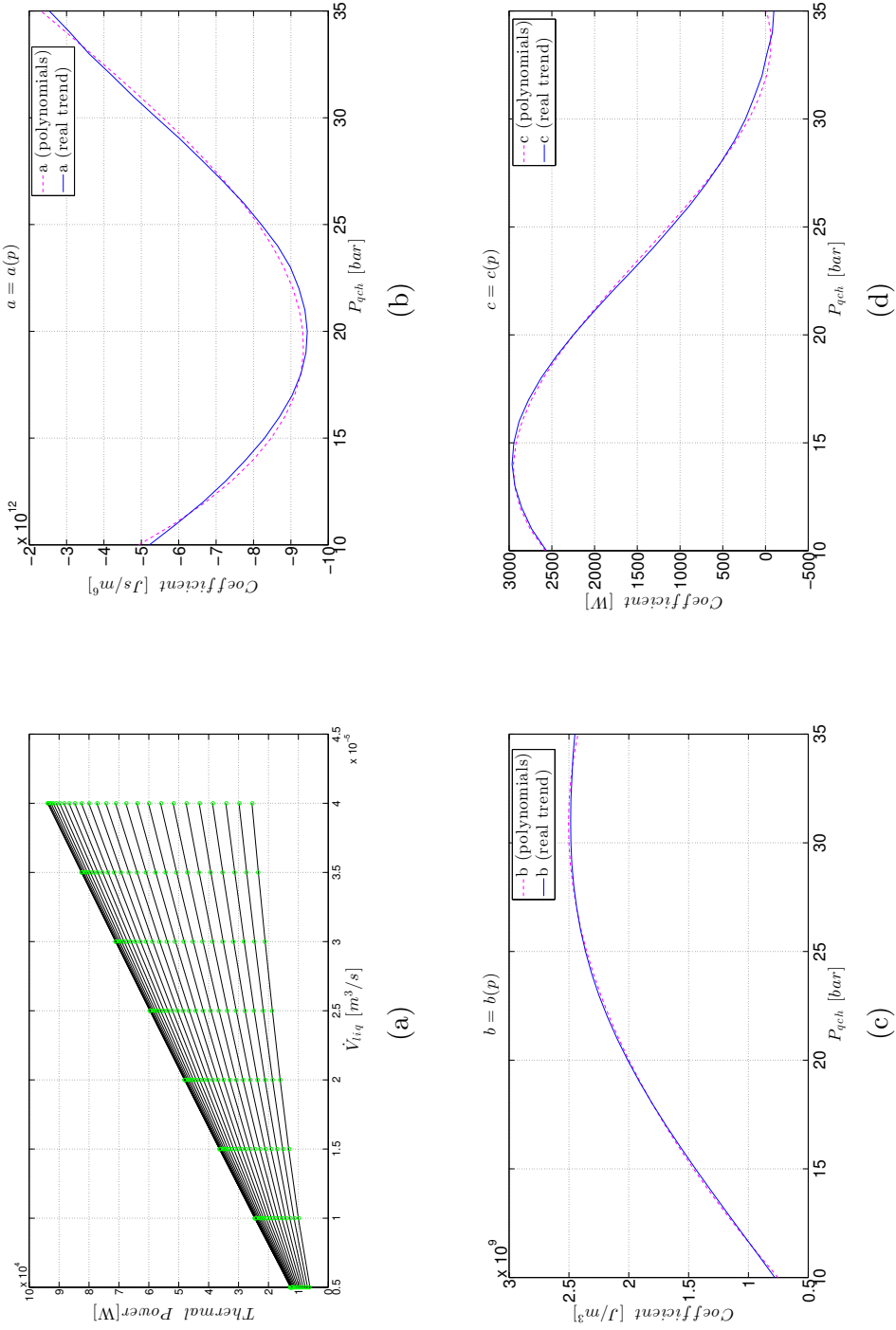


Figure 6.14 Analysis of the coefficients a , b and c

The units for a , b and c are Js/m^6 , J/m^3 and W , respectively. The validity of these expressions is shown at Figure 6.14 in which four graphics are present: Figure 6.14a shows the thermal power as a function of the cooling water flow rates; the interpolation poles needed to define f (green circles) are highlighted. Figures 6.14b to 6.14d compare the coefficient behavior estimated from our predictions with the same behavior evaluated from the developed third-degree polynomials. As it can be seen, the behavior of the coefficients a , b and c is close to the one evaluated using the polynomials, which allow us to argue that the error committed in using these expressions is negligible.

6.4.2 Definition of ψ

Let us define a coefficient ψ as a multiplicative factor which corrects the predictions of the developed model. Since it is a multiplicative coefficient, it can be also defined as the ratio between the predictions and the experimental data for given pressure and flow rate.

An analysis of Figure 6.7 to 6.9 clearly shows that, for a given quenching chamber pressure, the difference between the predictions and the experimental data is approximately constant and does not depend on the cooling water flow rate. For this reason, we assumed that the correction factor is a function of the quenching chamber pressure:

$$\psi = \psi(\mathbf{p}), \quad \mathbf{p} = \frac{p}{p_{max}}$$

In Table 6.2 we summarize the ratio between the predictions and the data for three quenching chamber pressures. Knowing these values, it is possible to find the second degree

Table 6.2 Ratios between predictions and data for three working pressures

Pressure	Ratios
$P_{qch} = 1.6MPa$	1.09
$P_{qch} = 2.1MPa$	0.881
$P_{qch} = 3.1MPa$	0.7549

polynomial which interpolates the aforementioned ratios. This operation is shown in Figure 6.15 and the mathematical expression given by:

$$\psi(\mathbf{p}) = 3.0933\mathbf{p}^2 - 4.5253\mathbf{p} + 2.4041 \quad (6.5)$$

Finally, in order to validate the proposed methodology, we plotted in Figure 6.16 the experimental data and the predictions using the correction factor. As it can be seen, the agreement is satisfactory. However, it is important to underline the limits of validity of the

presented expressions. Since we used polynomial interpolation, the aforementioned expressions should not be used for pressure lower than 16 *bar* or higher than 31 *bar*. That is, using the polynomial interpolations in the range of pressure in which these have been evaluated will avoid interpolation errors which raise close to the interpolation end nodes (where the error get worse).

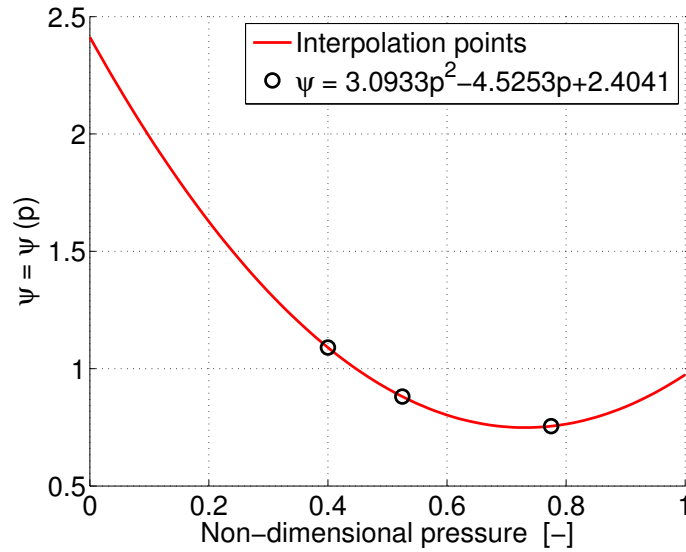


Figure 6.15 Evaluation of the correction coefficient (Equation 6.5)

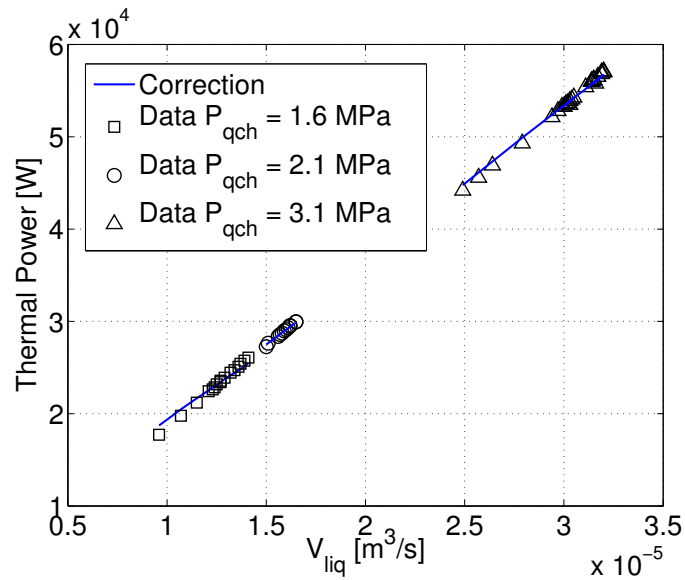


Figure 6.16 Experimental data and proposed correction on predictions

6.5 Final Remarks

The analysis made in this chapter gave us the possibility to review the modeling approach presented in Chapter 4 and 5. First, we have analyzed a single working condition in order to understand the physics of liquid droplets and we noted that a non-negligible portion of the droplets (i.e., the biggest ones) do not exchange all their energy. We justified this behavior by considering that they rapidly reach the bottom of the quenching chamber without completely vaporizing. Then, we compared the predictions with the experimental data and we found a good agreement at low pressures and an over estimation at higher ones. In effect, we assumed the occurrence of a other interactions between droplets and the quenching chamber. That is, droplets impact the inner wall of the chamber, forming a liquid layer that decreases the contact surface area and in turn, the heat transfer. Thereafter, we analyzed the possibility of having a combination of the flow rate and pressure that maximizes the performance of the DCHX. Studying the effects of these two parameters, we discovered that working at high pressures may not be advisable. Finally, in order to use our results, we computed polynomials capable of describing the model behavior and a factor which corrects the predictions. In this way, it will be possible to test our model for different values of the pressure and flow rate.

CHAPTER 7

CONCLUSION

During these two years, the quenching chamber used in a super-critical water loop facility installed at the “Altan Tapucu” Thermo-hydraulic Laboratory has been studied. The main function of this component is to cool down steam coming from the test section where super-critical choked flow conditions occur.

Here we summarize the main aspects of this study, in particular, the methodology used to solve the problems and its validation. In the end, we will present the utility of the results and the further works needed to improve our modeling approach.

7.1 General Objectives

Since the quenching chamber is a direct contact heat exchanger, this component does not present any particular complexity, because of the lack of a wall that divides both streams. In fact, it is a vertical vessel in which steam flows mixing with sub-cooled liquid. However, this equipment cases a nozzle located on the top of the tube. Due to this component, the cooling liquid enters into the chamber under the form of tiny droplets. This way, the contact surface area and, consequently, the thermal power, are maximized. The major problem analyzed in this work was the evaluation of the thermal power for given set of thermodynamic conditions of both streams (liquid and vapor). The solution was found by analyzing each of the following sub problems:

- **The thermodynamic evolution in the test section** the super-critical water passing through the test section is subjected to a considerable change in thermodynamic properties. This fact makes it difficult to evaluate the steam conditions entering the quenching chamber. In order to solve this problem, we assumed that the steam temperature is equal to the average between the temperature coming from an isentropic transformation and the one evaluated if the test section is an isenthalpic valve (Equation 5.1).
- **The evaluation of a statistical distribution for droplet size** the DDF is a parameter difficult to compute since it is a function of the working conditions (liquid temperature, steam pressure and volumetric flow rate) and of the geometric characteristics of the nozzle (the orifice diameter and the swirl-chamber length). All these variables have been taken into account by using an experimental correlation for the Sauter

- mean diameter (D_{32}). This parameter is needed in order to use the DDFs available in the scientific literature. Among all, the easiest DDF to handle is the Rosin-Rammler distribution which depends on D_{32} (Equation 4.5) and the exponent q of Equation 4.14.
- **Solution of the heat transfer problem for a single droplet** the evaluation of the droplet size is mandatory to perform the heat transfer study. Since there is a mutual interaction between super-heated steam and sub-cooled water, two heat transfer modes have been analyzed: convection and evaporation.
 - **Evaluation of the exchanged thermal power** finally, the results provided by the statistical and heat transfer studies (respectively in Chapter 4 and 5) have been used to compute the total power exchanged for a given DCHX condition. It was assumed that the latter quantity is equal to the total energy released by the droplets multiplied by the rate of droplets (Equation 5.18).

All these considerations have been used to develop a Matlab [®] script capable of not only computing the thermal power exchanged into the DCHX but also able to describe the behavior of droplets having different sizes and in a gaseous environment.

7.2 Limits of the Proposed Model

In the proposed modeling approach, some assumptions have been made to simplify the calculations. Their validity has been explained in the course of this work and shall be recapitulated here.

The methodology used to evaluate the DDF is questionable on several points. First of all, the experimental correlation used to evaluate the Sauter mean diameter (Equation 4.5) was found by Lefebvre (1989) under laboratory conditions extremely different from ours. For instance, Lefebvre used six different hollow-cone nozzles instead of a full cone nozzle. However, the theoretical assumptions used to develop this correlation were found to be always valid and independent from the type of nozzle considered (see Appendix A). This encouraged us to use Lefebvre's correlation. Secondly, even the use of the Rosin-Rammler equation may not be advisable since in the course of this work, we mentioned other statistical laws available in the scientific literature and it has been proven that these laws are more powerful than the Rosin-Rammler equation (Ashgriz, 2011). However these laws are also more difficult to use since they require the search of more than two statistical parameters. In effect, the lack of experimental data forces us to use the easiest statistical law available.

The heat transfer study was implemented following the theory as much as possible. In fact, if the convective heat transfer study is rigorous, the phase change solution is questionable since we did not provide any satisfactory reasons to explain the occurrence of liquid evaporation

instead of steam condensation. Moreover, even if the hypothesis of liquid evaporation is verified, we cannot exclude other phase change phenomena as, for instance, the evaporation of a liquid layer on the inner wall of the chamber. However, as it has been shown, taking into account these phenomena leads to a problem difficult to solve (Cascella and Teyssedou, 2013) and, at the same time, impossible to validate since there are no instruments capable of validating these assumptions. For these reasons, we limited ourselves to droplet evaporation only.

There are two more phenomena, namely the droplet break-up and collision that have not been considered in the model but we think that this assumption has a great influence on the model. Indeed, it affects the DDF shape since adding the two aforementioned phenomena increases the probability of having littler droplets. That is, in our work we considered only the decreases in droplet size due to evaporation, and not the ones due to break-up and collision. Moreover, they affect even the heat transfer calculations since break-up and collision are disruptive phenomena (Cascella and Teyssedou, 2013) which should increase the energy exchanged by the droplets. In scientific literature, we did not find any satisfactory model predicting these two phenomena and for this reason, we decide to neglect them. However, this decision is questionable.

Finally, we mentioned how the total rate of droplets may influence the thermal power calculations (Equation 5.18). Equation 5.22 shows that the total number of droplets can be evaluated by assuming all the droplets to have a diameter equal to the mean diameter associated to the DDF (Equation 4.14). Obviously, this assumption brings an error of which we cannot quantify the magnitude because of the lack of an instrument capable to measure the effective mean droplet size.

7.3 Result Discussion

As shown in Figure 6.6, our code describes well the heat exchange in the quenching chamber at low pressures but it over predicts the data at high pressures. We tried to justify this behavior by analyzing the dynamics of liquid droplets. Thus, we looked for all the phenomena that can influence our calculations.

Before performing the code, we were well aware of the fact that neglecting droplet break-up and collision affects the calculations. However, a preliminary analysis on these phenomena may help to understand their influence on the numerical predictions. Let us consider droplet break-up, which occurs when the surface tension is not high enough to contain the liquid instabilities. Recalling that the surface tension decreases with temperature, we can assume that the probability that a droplet will break up is higher at higher temperatures (and,

indeed, at higher pressures). Moreover, since break-up is a disruptive phenomenon, it should increase the heat transfer and this augmentation must be higher at higher pressures. The fact that we have an overestimation of the data at high pressures (Figure 6.6) brings us to conclude that including the break-up process may not necessarily improve the calculations. A similar analysis can be done for collision: the collision between two (or more) droplets leads to the formation of smaller droplets or of a larger droplet. Neglecting the last scenario, we can assume that the collision process augments the heat exchange since it increases the formation of tinier droplets. Hence, including collision process may not improve our model. This preliminary analysis leads us to consider other phenomena that may explain the behavior shown in Figure 6.6.

Another aspect affecting the model is the choice of q in Equation 4.14. We have shown that this parameter describes the shape of the DDF and has a great influence on the calculations. To understand how this variable affects the predictions, we have repeated the calculations for three values of q . In effect, we have found that the error increases with increasing q at low pressures but not at high ones. As shown in Figure 6.6, q has been chosen in such a way as to minimize the error between experimental data and numerical predictions. However, this is not a sufficient condition that can completely explain the discrepancy between the predictions and the data.

For these reasons, we have analyzed the behavior of droplets in the quenching chamber. We have assumed that they could impact the inner wall of our cylindrical vessel, forming a liquid layer which moves downward. Assuming this layer to be at saturation temperature, it should evaporate. In this scenario, the contact droplet surface area available to exchange heat decreases. Moreover, in Figure 6.5 we have stated that the heat transfer is a linear function of the surface area. If both of these hypotheses are correct, we can assume that the thickness of the liquid layer increases with pressure which in turn leads to a decrease in the total droplet-surface area (and so, the heat transfer). Finally, we can assume that this behavior is more important at high pressures, and not at low ones, which may explain the gap between the predictions and the data shown in Figure 6.6.

7.4 Usefulness of the Proposed Model

Even if we were not able to propose a satisfactory model (i.e., which well describes the quenching chamber behavior over a wide range of pressures), doing so gave us the possibility to better understand the dynamics of liquid droplets in a steam environment. In fact, in this model, the physical parameters linked to the droplet (i.e., the size, the residence time and the velocity) have been used to evaluate the overall heat transfer.

based on the proposed theoretical approach, we were able to demonstrate that the quenching chamber (and probably all DCHXs of this type) admits a set of working conditions which maximize its performance. This aspect has been exposed in different sections of this document

In Figure 6.5 we have analyzed the heat transfer as a function of droplet size; two aspects have been highlighted. Firstly, the energy released grows linearly with the contact surface area (which is obvious). Secondly, there is a decrease in the amount of energy released due to the impact of some droplets (i.e., the bigger ones) on the bottom of the chamber. In fact, their velocity is too high and they are not able to completely vaporize. Hence, we assumed the existence of a minimal volumetric flow rate that makes all the droplets change their phase and, consequently, maximizes the amount of heat transferred. In Figure 6.10, the effect of q on Equation 4.14 has been analyzed for a given volumetric flow rate. Even in this case, we found a pressure which maximizes the heat transfer. Because of that, a further analysis on the statistics of liquid droplets should be done, in order to compute the real value of q to be used. Finally, the analysis of Figure 6.12 and Figure 6.13 leads us to conclude that two parameters, namely the chamber pressure and volumetric flow rate affect significantly our calculations. The parametric study shows that the heat transfer grows linearly with the flow rate but not with the pressure. In fact, increasing the latter for a given flow rate leads to an asymptotic value of the heat transfer. For this reason, we stated that working at high pressures is not advisable since the only way to increase the heat transfer is by increasing the water rate.

This analysis has helped to understand the behavior of a DCHX. Obviously, we cannot forget that the predictions may not always be true but, if the code forecasts the right trends (i.e., there is a working condition maximizing the performances), the way of designing these heat exchangers will be revised. We underline that these systems find applications not only in heat exchangers, chemical reactors and agriculture factories, but even in nuclear engineering (depressurizers) and fire extinguishers, fields in which safety is a mandatory requirement. If our assumptions are correct, the implementation of this code (and any future improvement) will help to increase the efficiency of these systems and in turn their safety.

7.5 Future Work

In the course of this work we have often highlighted the weak points of our modeling approach. For this reason, any future improvement of the presented methodology cannot neglect these points.

It is obvious that further work is needed to provide a better way to compute the DDF.

The equation used to estimate D_{32} must be adapted to the type of spray nozzle and the use of other DDFs should be considered as well. It is clear that this kind of improvement requires the use of additional experimental data (i.e., the direct measure of the droplet sizes).

We often mentioned droplet break-up and collision. In fact, they have been neglected in our work but these phenomena have a great influence on the quenching chamber behavior and any improvement of the code cannot neglect these factors. At first glance they may deteriorate the performances of the proposed model. However, the results obtained by introducing these phenomena will be different from the ones showed here and their analysis may be easier to explain.

Another assumption is the formation of a liquid layer on the inner wall of the quenching chamber. Since droplets feed this layer, these will impact the wall at different locations. This means that another information should be evaluated which is the moving directions of the droplets. Knowing their size should make it possible to evaluate the direction under which droplets move and consequently, determine those droplets that impact the cylindrical wall of the DCHX.

We highlighted certain aspects that were neglected and the relation they have on the dynamics of the liquid droplets. We can underline another aspect related to the behavior of the quenching chamber. In fact, our calculations have shown the existence of a set of working conditions that can maximize the performance. It would be interesting to prove this fact since, once achieved, it will have a great influence on the way these type of thermal equipment are designed. For these reasons, further *ad hoc* experiments should be implemented in order to validate the behavior shown in Figure 6.12 and 6.13.

Finally, we underlined that, when developing the proposed model, several assumptions have been made because of the lack of an optical instrument capable of showing the droplet behavior within the quenching chamber. For instance, we assumed the droplet size to be described by the Rosin-Rammler distribution or the formation of an evaporating liquid layer on the inner wall of the DCHX. All these assumptions, including the others not listed here, can easily be validated by the introduction of a measurement instrument such as a camera or an image analyzer.

REFERENCES

- ASHGRIZ, N. (2011). *Handbook of Atomization and Sprays: Theory and Applications*. Springer.
- BARRERAS, F. and EDUARDO, L. (2006). Experimental Characterization of Industrial Twin-Fluid Atomizers. *Atomization Spray J. Inst. Liq. Atomization Spray Syst.*, vol. 16, pp. 127–145.
- BECK, J. C. and WATKINS, A. P. (2002). On the Development of Spray Submodels Based on Droplet Size Moments. *Journal of Computational Physics*, vol. 182, pp. 586–621.
- BRONIARZ-PRESS, L., OCHOWIAK, M., ROZANSKI, J. and WOZIWODZKI, S. (2009). The Atomization of Water-Oil Emulsions. *Exp. Thermal Fluid Sci.*, vol. 20, pp. 631–637.
- CARSLAW, H. S. (1959). *Conduction of Heat in Solids*. Oxford : Clarendon Press.
- CASCELLA, F. and TEYSSEDOU, A. (2013). Modeling a direct contact heat exchanger for supercritical water loop. *Proceedings of the 2013 Canadian Nuclear Society Annual Conference, Toronto, 12/06/2013*.
- CELATA, G. P., CUOMO, M., D'ANNIBALE, F. and FARELLO, G. E. (1991). Direct Contact Condensation of Steam on Droplets. *Int. J. Multiphase Flow*, vol. 17, pp. 191–211.
- CLEARY, V., BOWEN, P. and WITLOX, H. (2007). Flashing Liquid Jets and Two-Phase Droplet Dispersion: 1. Experiments for derivation of droplet Atomization Correlation. *J. Hazard. Mater.*, vol. 142, pp. 786–796.
- CROWE, C. T. (2005). *Multiphase Flow Handbook*. CRC Press.
- GONZÁLES-TELLO, P., CAMACHO, F., VICARIA, J. M. and GONZÁLES, P. A. (2008). A Modified Nukiyama-Tanasawa Distribution Function and a Rosin-Rammler Model for the Particle-Size-Distribution Analysis. *Powder Technology*, vol. 186, pp. 278–281.
- HUANG, L. J., AYYASWAMY, P. S. and SRIPADA, S. S. (1996). Condensation on a Spray of Water Drops: a Cell Model Study–II. Transport Quantities. *Int. J. Heat Mass Transfer*, vol. 39, pp. 3791–3797.
- INCROPERA, F. P., DEWITT, D. P., BERGMAN, T. L. and LAVINE, A. S. (2007). *Fundamentals of Heat and Mass Transfer*. Wiley.
- JACOBS, H. R. (2011). *Direct Contact Heat Exchangers*. Thermopedia. <http://www.thermopedia.com/content/700/>.
- LEFEBVRE, A. H. (1989). *Atomization and Sprays*. Hemisphere Publishing Corp.

- MARSHALL, W. R. (1955). Heat and Mass Transfer in Spray Drying. *Transaction of ASME*, pp. 1377–1385.
- MUFTUOGLU, A. and TEYSSEDOU, A. (2013). Experimental study of water flow at supercritical pressures. *Proceedings of the 2013 Canadian Nuclear Society Annual Conference, Toronto, 12/06/2013*.
- ORZECZOWSKI, A. (1976). *Liquid Atomization*. WNT, Warsaw.
- OZISIK, M. N. (1993). *Heat Conduction*. John Wiley & Sons, Inc.
- RANZ, W. E. and MARSHALL, W. R. (1952). Evaporation from Drops. *Chemical Engineering Progress*, vol. 48, pp. 141–146, 173–180.
- ROSIN, P. and RAMMLER, E. (1933). The Laws Governing the Fineness of Powdered Coal. *Journal of the Institute of Fuel*, vol. 7, pp. 29–36.
- SAUNDERS, E. A. (1988). *Heat Exchanges: Selection, Design and Construction*. Longman Scientific and Technical.
- SCHICK, R. J. (2006). *Spray Technology Reference Guide: Understanding Drop Size*. Spraying Systems Co. <http://de.spray.com/Portals/0/pdf/B459c.pdf>.
- SCHNEIDER, P. J. (1955). *Conduction Heat Transfer*. Addison-Wesley Publishing Company, Inc.
- SEMIAO, V., ANDRADE, P. and DE GARCA CARVALHO, M. (1996). Spray Characterization: Numerical Prediction of Sauter Mean Diameter and Droplet Size Distribution. *Fuel*, vol. 75, pp. 1707–1714.
- SRIPADA, S. S., AYYASWAMY, P. S. and HUANG, L. J. (1996). Condensation on a spray of water drops: A cell model study—I. Flow description. *Int. J. Heat Mass Transfer*, vol. 39, pp. 3781–3790.
- TAKAHASHI, M., NAYAK, A. K., KITAGAWA, S. and MURAKOSO, H. (2001). Heat Transfer in Direct Contact Condensation of Steam to Subcooled Water Spray. *Journal of Heat Transfer*, vol. 123, pp. 703–710.
- ZHAO, Y. H., HOU, M. H. and CHIN, J. S. (1986). Droplet Size Distributions for Swirl and Airblast Atomizers. *Atomization Spray Technol.*, vol. 2, pp. 3–15.

APPENDIX A

Development of an experimental correlation for D_{32} (Lefebvre, 1989)

In Chapter 4, we showed that the knowledge of the Sauter mean diameter defined as

$$SMD = \frac{\sum_{i=1}^N n_i D_i^3}{\sum_{i=1}^N n_i D_i^2}$$

is fundamental to evaluate the DDF. In our modeling approach, we used the experimental correlation found by Lefebvre (1989). We summarize here the theory behind the development of this correlation.

The droplet size is strictly correlated to the atomization process defined as “the conversion of bulk liquid issuing from a nozzle into a dispersion of small droplets ranging in size from sub micron to several hundred microns in diameter” (Jacobs, 2011). In Figure .1 this conversion is showed: the liquid gets out from the nozzle but it is in a continuous phase; then, because of the aerodynamic and hydrodynamic instabilities, the liquid sheet breaks up into ligaments and then into droplets.

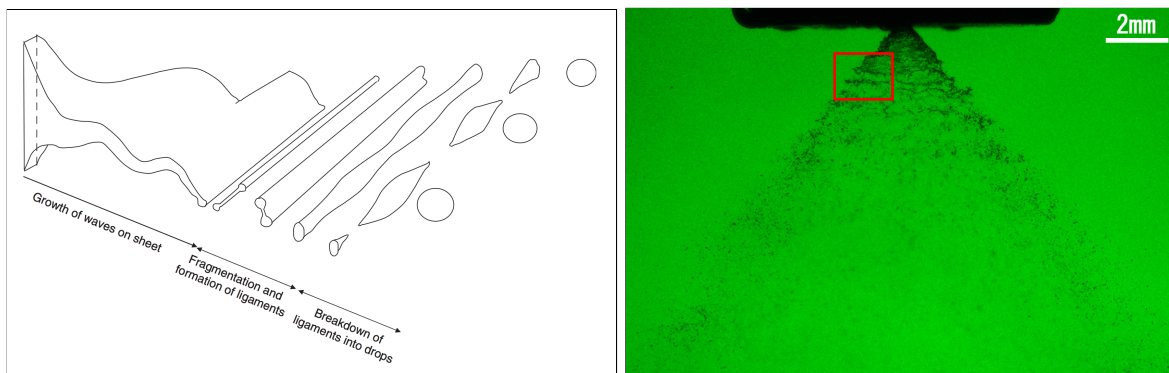


Figure .1 Atomization Process

The main idea explained in Lefebvre (1989) is to develop an experimental correlation for D_{32} which is the sum of two terms:

- the first term is related to the first stage of atomization, where hydrodynamic and aerodynamic forces generate instabilities into the liquid sheet;

- the second term is related to second stage of atomization where the liquid passes from a continuous to a disperse phase (conversion of the liquid sheets into ligaments and then into droplets).

That is, an expression of the following form is to be found

$$D_{32} = D_{32,1} + D_{32,2} \quad (1)$$

Respectively, $D_{32,1}$ and $D_{32,2}$ are function of the two aforementioned stages.

1st atomization In the first stage, the disruptive forces take place into the liquid sheet: this force is related to the volumetric flow and consequently to the initial liquid velocity. The stronger the force, the lower the droplet size becomes. Moreover, in order to have a better atomization quality, the liquid viscosity must decrease. These considerations allow us to write a dependence of the Reynolds number Re on $D_{32,1}$

$$\frac{D_{32,1}}{t_s} \propto Re^{-x} \quad Re = \frac{\rho_L v_L t_s}{\mu_L}$$

t_s is the liquid sheet length and v_L the liquid velocity. Another aspect affecting the droplet size is the ratio between the aerodynamic forces acting on liquid surface to the surface tension. That is, $D_{32,1}$ is inversely proportional to the Weber number:

$$\frac{D_{32,1}}{t_s} \propto We^{-0.5x} \quad We = \frac{\rho_v t_s v_R^2}{\sigma}$$

with v_R the relative velocity between the liquid and the gaseous media. The first term of Equation 1 can be written as

$$\frac{D_{32,1}}{t_s} \propto (Re \sqrt{We})^{-x} \rightarrow D_{32,1} \propto \left(\frac{\sigma^{0.5} \mu_L}{\rho_v^{0.5} \rho_L v_R v_L} \right)^x (t \cos \theta)^{1-1.5x}$$

θ is half the cone spray angle and $t_s = t \cos \theta$.

2nd atomization In order to have a finer atomization, the surface tension σ must be low, and the relative velocity v_R must be high:

$$\frac{D_{32,2}}{t_s} \propto We^{-y} = \left(\frac{\sigma}{\rho_v t_s v_R^2} \right)^y \rightarrow D_{32,2} \propto \left(\frac{\sigma}{\rho_v v_R^2} \right)^y (t \cos \theta)^{1-y}$$

Recalling Equation 1, we can write

$$D_{32} = A \left(\frac{\sigma^{0.5} \mu_L}{\rho_v^{0.5} \rho_L v_R v_L} \right)^x (t \cos \theta)^{1-1.5x} + B \left(\frac{\sigma \rho_L}{\rho_v v_R^2} \right)^y (t \cos \theta)^{1-y}$$

Assuming $v_R \simeq v_L$ and $\Delta P_L = 0.5 \rho_L v_L^2$

$$D_{32} = A \left(\frac{\sigma^{0.5} \mu_L}{\rho_v^{0.5} \Delta P_L} \right)^x (t \cos \theta)^{1-1.5x} + B \left(\frac{\sigma \rho_L}{\rho_v \Delta P_L} \right)^y (t \cos \theta)^{1-y}$$

Lefebvre (1989) analyzed the behavior of six simplex hollow-cone atomizers of different size and spray-cone angle ($60 < \theta < 90$); the working fluids were water, diesel oil and blend of diesel oil with polybutene. Experiments performed by Lefebvre allowed him to find the following constants:

$$x = 0.5, \quad y = 0.25, \quad A = 4.52, \quad B = 0.39$$

Finally, Lefebvre (1989) proposed a correlation to find the normal liquid sheet length, necessary parameter to compute D_{32} :

$$t = 2.7 \left[\frac{d_0 FN \mu_l}{(\rho_l \Delta P_l)^{0.5}} \right]^{0.2}$$

where d_0 is the discharge orifice diameter and FN is the flow number:

$$FN = \frac{\dot{m}_l}{(\rho_l \Delta P_l)^{0.5}}$$

\dot{m}_l is the liquid flow rate [kg/s].

APPENDIX B

Solution of the Heat Transfer Problem – Convection

The conduction equation in spherical coordinates has been used in order to find the droplet mean temperature. The complete three-dimensional (r, θ, ϕ) homogeneous equation is

$$\frac{\partial^2 T}{\partial r^2} + \frac{2}{r} \frac{\partial T}{\partial r} + \frac{1}{r^2 \sin \theta} \frac{\partial}{\partial \theta} \left(\sin \theta \frac{\partial T}{\partial \theta} \right) + \frac{1}{r^2 \sin^2 \theta} \frac{\partial^2 T}{\partial \phi^2} = \frac{1}{\alpha} \frac{\partial T}{\partial t}$$

Neglecting the effect of the polar angle θ and the azimuth angle ϕ , the dependence of the radius r on T can be written as

$$\frac{\partial^2 T}{\partial r^2} + \frac{2}{r} \frac{\partial T}{\partial r} = \frac{1}{\alpha} \frac{\partial T}{\partial t}$$

or

$$\frac{1}{r} \frac{\partial^2}{\partial r^2} (rT) = \frac{1}{\alpha} \frac{\partial T}{\partial t} \quad (2)$$

with the following boundary conditions

$$\begin{aligned} \left. \frac{\partial T}{\partial r} \right|_{r=0} &= 0 \\ T(r, 0) &= T_i \\ -k_l \left. \frac{\partial T}{\partial r} \right|_{r=R} &= h[T_\infty - T(R, t)] \end{aligned}$$

To solve this problem, the following change of variable is applied. This leads to a differential equation easier to handle

$$\Theta(r, t) = rT(r, t)$$

So, Equation 2 becomes

$$\frac{\partial^2 \Theta(r, t)}{\partial r^2} = \frac{1}{\alpha} \frac{\partial \Theta(r, t)}{\partial t} \quad (3)$$

The new boundary conditions to solve Equation 3 are

$$\begin{aligned} \left. \frac{\partial \Theta}{\partial r} \right|_{r=0} &= \lim_{r \rightarrow 0} \frac{\Theta(r, t)}{r} \\ \Theta(r, 0) &= rT_i = \Theta_i \\ -k_l \left. \frac{\partial \Theta}{\partial r} \right|_{r=R} &= \Theta(R, t) \left(h + \frac{k_l}{R} \right) \end{aligned}$$

Where the limit of the first boundary condition exists and is finite. Following the method of the separation of variables, we assume that the function $\Theta(r, t)$ can be written as

$$\Theta(r, t) = \rho(r) \tau(t)$$

leading to the search of the functions ρ and τ . Introducing these two functions, Equation 3 becomes

$$\frac{1}{\rho(r)} \frac{d^2 \rho(r)}{dr^2} = \frac{1}{\alpha \tau(t)} \frac{d\tau(t)}{dt} = -\zeta^2 \quad (4)$$

So, the following equation can be written

$$\frac{d\tau(t)}{dt} + \alpha \zeta^2 \tau(t) = 0$$

which has a solution of the form

$$\tau(t) = A e^{-\alpha \zeta^2 t}$$

with A a constant to be determined. Here we understand the negative sign before ζ^2 in Equation 4 : that way, we avoid a solution for τ that diverges to infinity since α , ζ^2 and t are always positive quantities. The function $\rho(r)$ comes from

$$\frac{d^2 \rho(r)}{dr^2} + \zeta^2 \rho(r) = 0$$

The solution has the following form

$$\rho(r) = C_1 \cos(\zeta r) + C_2 \sin(\zeta r) \quad (5)$$

where the two constants have to be determined from the boundary conditions. So,

$$\left. \frac{\partial \Theta}{\partial r} \right|_{r=0} = \lim_{r \rightarrow 0} \frac{\Theta(r, t)}{r} = \lim_{r \rightarrow 0} \frac{\tau(t)}{r} [C_1 \cos(\zeta r) + C_2 \sin(\zeta r)] = \lim_{r \rightarrow 0} \tau(t) \left[\frac{C_1}{r} + C_2 \zeta \frac{\sin(\zeta r)}{\zeta r} \right]$$

The limit goes to infinity for $r \rightarrow 0$; in order to avoid a prediction of an infinite temperature in the center of the droplet, we impose $C_1 = 0$. So, the solution of the problem has the form

$$\rho(r) = \rho(\zeta, r) = C_2 \sin(\zeta r)$$

Applying the boundary condition of the heat transfer on the droplet surface we obtain

$$1 - R\zeta \cot R\zeta = \frac{hR}{k_l} = Bi$$

with Bi the Biot number. Equation 7.5 has infinite roots so, $\zeta = \zeta_n$. Introducing $C = AC_2$, the solution of the problem is

$$\Theta(r, t) = \sum_{n=1}^{\infty} \tau(t, \zeta_n) \rho(r, \zeta_n) = \sum_{n=1}^{\infty} C e^{-\alpha \zeta_n^2 t} \sin(\zeta_n r)$$

The evaluation of C comes from the application of the initial constant temperature to the obtained solution:

$$\Theta_i = rT_i = \sum_{n=1}^{\infty} C \sin(\zeta_n r)$$

leading to

$$C_n = \frac{1}{N(\zeta_n)} \int_0^R \rho(r, \zeta_n) rT_i dr \quad \text{since} \quad \forall n \exists! C_n$$

With $N(\zeta_n)$ the norm, defined as

$$N(\zeta_n) = \int_0^R \rho(r, \zeta_n) \rho(r, \zeta_m) dr$$

which is different of zero for $m = n$. So, C_n becomes

$$C_n = \frac{1}{\int_0^R \sin(r, \zeta_n) dr} \int_0^R \sin(r, \zeta_n) rT_i dr = \frac{4\zeta_n [T_i \sin \zeta_n R - \zeta_n R \cos \zeta_n R]}{2R\zeta_n - \sin 2\zeta_n R}$$

The final solution of the equation is

$$\Theta(r, t) = \sum_{n=1}^{\infty} e^{-\alpha \zeta_n^2 t} \frac{4\zeta_n [T_i \sin \zeta_n R - \zeta_n R \cos \zeta_n R]}{2R\zeta_n - \sin 2\zeta_n R} \sin(\zeta_n r)$$

Or, introducing the non-dimensional temperature $\frac{T(r,t)-T_\infty}{T_i-T_\infty}$, the Fourier number $Fo = \frac{\alpha t}{R^2}$ and the non-dimensional radius $\mathbf{r} = \frac{r}{R}$, we obtain the temperature trend in a more elegant form:

$$\frac{T(r, t) - T_\infty}{T_i - T_\infty} = \sum_{n=1}^{\infty} \frac{4[\sin \zeta_n - \zeta_n \cos \zeta_n]}{2\zeta_n - \sin 2\zeta_n} e^{-\zeta_n^2 Fo} \frac{\sin \zeta_n \mathbf{r}}{\zeta_n \mathbf{r}}$$

APPENDIX C

First Five Roots of Transcendental Equation 5.9 (Schneider, 1955)

$$1 - \zeta_n \cot \zeta_n = Bi$$

Bi	ζ_1	ζ_2	ζ_3	ζ_4	ζ_5
0	0	4.4934	7.7253	10.9041	14.0662
0.005	0.1224	4.4945	7.7259	10.9046	14.0666
0.01	0.173	4.4956	7.7265	10.905	14.0669
0.02	0.2445	4.4979	7.7278	10.906	14.0676
0.03	0.2991	4.5001	7.7291	10.9069	14.0683
0.04	0.345	4.5023	7.7304	10.9078	14.069
0.05	0.3854	4.5045	7.7317	10.9087	14.0697
0.06	0.4217	4.5068	7.733	10.9096	14.0705
0.07	0.4551	4.509	7.7343	10.9105	14.0712
0.08	0.4860	4.5112	7.7356	10.9115	14.0719
0.09	0.515	4.5134	7.7369	10.9124	14.0726
0.1	0.5423	4.5157	7.7382	10.9133	14.0733
0.2	0.7593	4.5379	7.7511	10.9225	14.0804
0.3	0.9208	4.5601	7.7641	10.9316	14.0875
0.4	1.0528	4.5822	7.777	10.9408	14.0946
0.5	1.1656	4.6042	7.7899	10.9499	14.1017
0.6	1.2644	4.6261	7.8028	10.9591	14.1088
0.7	1.3525	4.6479	7.8156	10.9682	14.1159
0.8	1.432	4.6696	7.8284	10.9774	14.123
0.9	1.5044	4.6911	7.8412	10.9865	14.1301
1	1.5708	4.7124	7.8540	10.9956	14.1372
1.5	1.8366	4.8158	7.9171	11.0409	14.1724
2	2.0288	4.9132	7.9787	11.0856	14.2075
3	2.2889	5.087	8.0962	11.1727	14.2764
4	2.4557	5.2329	8.2045	11.256	14.3434
5	2.5704	5.354	8.3029	11.3349	14.408
6	2.6537	5.4544	8.3914	11.4086	14.4699

7	2.7165	5.5378	8.4703	11.4773	14.5288
8	2.7654	5.6078	8.5406	11.5408	14.5847
9	2.8044	5.6669	8.6031	11.5994	14.6374
10	2.8363	5.7172	8.6587	11.6532	14.687
11	2.8628	5.7606	8.7083	11.7027	14.7335
16	2.9476	5.908	8.8898	11.8959	14.9251
21	2.993	5.9921	9.0019	12.025	15.0625
31	3.0406	6.0831	9.1294	12.1807	15.238
41	3.0651	6.1311	9.1987	12.2688	15.3417
51	3.0801	6.1606	9.242	12.3247	15.409
∞	3.1105	6.2211	9.3317	12.4426	15.5537

APPENDIX D

Determination of the experimental data

In Figure 6.6 we compared the thermal power predicted by our code and measured in the thermal facility (Figure 3.1). The data we plotted in Figure 6.6 have been indirectly evaluated applying an energy balance to the quenching chamber, i.e., the decrease in enthalpy at which the steam is subjected must be equal to the water enthalpy increase. Neglecting the thermal losses to the environment, we can write (Figure .1)

$$\dot{Q}_{qc,exp} = \dot{m}_2 (h_2 - h_3) = \dot{m}_1 (h_3 - h_1) \quad (6)$$

where \dot{m}_i is the mass flow rate and h_i is the enthalpy. The resolution of Equation 6 makes it possible to compute the thermal power exchanged $\dot{Q}_{qc,exp}$, evaluating either the enthalpy variation of the steam or the enthalpy variation of the liquid (expect for a sign change).

In order to use Equation 6, all the stream temperatures and flow rates (Figure .1) have to be estimated. This task is done by the measure instruments present in the experimental facility:

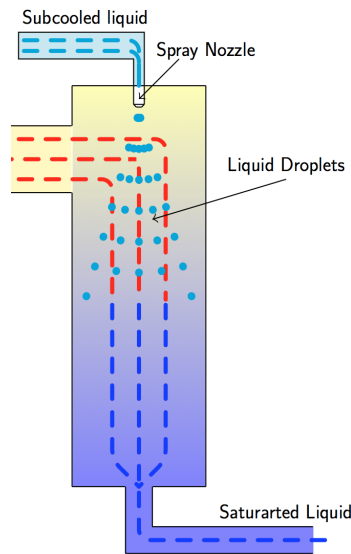


Figure .1 Quenching chamber scheme

- **Stream 1:** The thermodynamic conditions 1 can be exactly determined: in fact, a flow meter (technical designation “Flowmeter#2” in Figure 3.1) makes it possible to

measure the liquid flow rate, while the temperature comes from the measure of the thermocouple present at SCWL inlet (“TTr-8” technical designation in Figure 3.1).

- **Stream 2:** The conditions $\mathcal{2}$ of the steam entering in the DCHX are less easier to predict: the fact that the transformation occurring in the test section isn’t thermodynamically known makes it difficult to evaluate the steam flow rate and temperature. As it can be seen in Figure 3.1, there isn’t a flow meter at test section outlet. This means that any evaluation on steam flow rate should come from the flow meter identified with “Flowmeter#1” (Figure 3.1). However, choked flow conditions occurring in the test section makes this task hard. On the other hand, a thermocouple is set at test section outlet (“TTr-6” technical designation in Figure 3.1). However, this last has a time constant lower than other thermocouples present in the SCWL (i.e., “TTr-7” and “TTr-8”, which are electrical thermocouples). That is, using the information from “TTr-6” leads to an error in steam temperature evaluation, as it may happen in transient conditions (for instance, when the heater is turned off, the steam temperature decreases, but the thermocouple predicts an increase in steam temperature: obviously, this is meaningless).
- **Stream 3:** The conditions $\mathcal{3}$ at quenching chamber outlet can be partially determined: the stream temperature comes from the thermocouple identified with the “TTr-7” technical designation (Figure 3.1), while the lack of any flow meter at quenching chamber outlet makes difficult an evaluation on the mass flow rate.

Finally, an other important parameter to be known is the quenching chamber pressure: neglecting the pressure drop in the quenching chamber, we can assume that it is equal to the pressure at test section exit, where a pressure traducer is installed (not shown in Figure 3.1).

As it can be argued, only the liquid conditions are accurately known: for this reason, we used the last hand of Equation 6 to estimate $\dot{Q}_{qc,exp}$:

$$\dot{Q}_{qc,exp} = \underbrace{\dot{m}_1}_{\text{Flowmeter\#2}} \left(\underbrace{h_3}_{\text{TTr-7}} - \underbrace{h_1}_{\text{TTr-8}} \right)$$

We point out that the measurement from “TTr-7” isn’t necessary in our calculations: in fact, recalling the procedure presented in Chapter 5, the liquid change its phase to become vapor; this means that h_3 is equal to saturated-steam enthalpy h_v at the quenching chamber pressure P_{qch} . This assumption is supported by the fact that “TTr-7” provides always the saturation temperature at the working pressure P_{qch} .